Impact of the Madden–Julian Oscillation on the Indonesian Throughflow in the Makassar Strait during the CINDY/DYNAMO Field Campaign

TOSHIAKI SHINODA,[a] WEIQING HAN,[b] TOMMY G. JENSEN,[c] LUIS ZAMUDIO,[d] E. JOSEPH METZGER,[c] AND REN-CHIEH LIEN[e]

[a] *Texas A&M University–Corpus Christi, Corpus Christi, Texas*
[b] *University of Colorado Boulder, Boulder, Colorado*
[c] *Naval Research Laboratory, Stennis Space Center, Mississippi*
[d] *Florida State University, Tallahassee, Florida*
[e] *Applied Physics Laboratory, University of Washington, Seattle, Washington*

(Manuscript received 8 October 2015, in final form 29 April 2016)

ABSTRACT

Previous studies indicate that equatorial zonal winds in the Indian Ocean can significantly influence the Indonesian Throughflow (ITF). During the Cooperative Indian Ocean Experiment on Intraseasonal Variability (CINDY)/Dynamics of the Madden–Julian Oscillation (DYNAMO) field campaign, two strong MJO events were observed within a month without a clear suppressed phase between them, and these events generated exceptionally strong ocean responses. Strong eastward currents along the equator in the Indian Ocean lasted more than one month from late November 2011 to early January 2012. The influence of these unique MJO events during the field campaign on ITF variability is investigated using a high-resolution ($^1/_{25}°$) global ocean general circulation model, the Hybrid Coordinate Ocean Model (HYCOM). The strong westerlies associated with these MJO events, which exceed 10 m s^{-1}, generate strong equatorial eastward jets and downwelling near the eastern boundary. The equatorial jets are realistically simulated by the global HYCOM based on the comparison with the data collected during the field campaign. The analysis demonstrates that sea surface height (SSH) and alongshore velocity anomalies at the eastern boundary propagate along the coast of Sumatra and Java as coastal Kelvin waves, significantly reducing the ITF transport at the Makassar Strait during January–early February. The alongshore velocity anomalies associated with the Kelvin wave significantly leads SSH anomalies. The magnitude of the anomalous currents at the Makassar Strait is exceptionally large because of the unique feature of the MJO events, and thus the typical seasonal cycle of ITF could be significantly altered by strong MJO events such as those observed during the CINDY/DYNAMO field campaign.

1. Introduction

The Madden–Julian oscillation (MJO) produces significant ocean responses in the tropical Indian and Pacific Oceans, including upper-ocean currents, thermocline depth, and their propagation as equatorial waves (e.g., Kessler et al. 1995; Ralph et al. 1997; Waliser et al. 2003; Shinoda et al. 2008, 2013a). Previous studies suggest that these ocean variations in response to the MJO vary substantially from event to event (e.g., Shinoda and Hendon 2001; Cravatte et al. 2003; Roundy and Kiladis 2006).

During the Cooperative Indian Ocean Experiment on Intraseasonal Variability (CINDY)/Dynamics of the Madden–Julian Oscillation (DYNAMO) field campaign (Yoneyama et al. 2013; Zhang et al. 2013), exceptionally strong ocean responses, especially near the equator, were observed in the tropical Indian Ocean (e.g., Shinoda et al. 2013b; Gottschalck et al. 2013; Moum et al. 2013; Jensen et al. 2015). During the field campaign in fall 2011 and winter 2011/12, strong surface westerlies associated with large MJO events in late November and mid-December were observed. These events were unique in that the large-scale strong

Naval Research Laboratory Contribution Number NRL/JA/7320–15-2840.

Corresponding author address: Toshiaki Shinoda, Texas A&M University–Corpus Christi, 6300 Ocean Dr., Corpus Christi, TX 78412.
E-mail: toshiaki.shinoda@tamucc.edu

DOI: 10.1175/JCLI-D-15-0711.1

convection events in the Indian Ocean occurred within one month without a clear suppressed phase between them (Yoneyama et al. 2013). Consequently, relatively strong equatorial westerlies were observed most of the time in late November–December, and these wind anomalies generated strong eastward oceanic jets on the equator, which lasted more than one month. Such long-lasting strong equatorial jet can influence other parts of the ocean through oceanic wave propagation. For example, Shinoda et al. (2013b) demonstrated that these MJO events significantly influence remote areas of the Indian Ocean, including the center of Seychelles–Chagos thermocline ridge region (3°–10°S, ~60°E) through the propagation of reflected Rossby waves.

Previous studies indicate that anomalous equatorial zonal currents in the Indian Ocean could significantly influence the upper-ocean structure and circulation in the Indonesian seas (e.g., Clarke and Liu 1993; Masumoto and Yamagata 1993; Sprintall et al. 2000; Durland and Qiu 2003; Zhou and Murtugudde 2010; Schiller et al. 2010; Shinoda et al. 2012; Pujiana et al. 2013). These include the transport of Indonesian Throughflow (ITF), which is an important part of global thermohaline (''conveyor belt'') and wind-driven circulations, carrying upper-ocean waters from the Pacific to the Indian Ocean and contributing to maintaining upper-ocean circulations in the Indo-Pacific regions (e.g., Tilburg et al. 2001; Lee et al. 2002). For example, Shinoda et al. (2012) investigated the dynamical processes that control the seasonal variation of the ITF based on the analysis of the 1/12° grid global ocean general circulation model simulation. Shinoda et al. (2012) demonstrated that the reduction of ITF in May and October–November is primarily caused by the propagation of coastal Kelvin waves from the Indian Ocean, while rapid recovery of the transport during December–March is controlled mostly by the annual Rossby waves in the Pacific Ocean. During May and October, the eastward oceanic jet is generated on the equator in the Indian Ocean because of the reversal of zonal equatorial winds associated with the monsoon transition (Wyrtki 1973; referred to as ''Wyrtki jet'' hereafter). Previous studies also indicate that the intraseasonal variability of equatorial winds in the Indian Ocean significantly influence the ITF transport (Qiu et al. 1999; Schiller et al. 2010; Zhou and Murtugudde 2010; Pujiana et al. 2013). For example, Pujiana et al. (2013) suggested that the ITF transport at the Makassar Strait, which generally accounts for about 80% of the total ITF transport (Gordon 2005), is reduced up to 2 Sv (1 Sv $\equiv 10^6\,m^3\,s^{-1}$) by the intraseasonal wind event over the equatorial Indian Ocean and by Kelvin wave propagation.

In this study, the remote ocean response in the Indonesian seas to the unique MJO events observed during the CINDY/DYNAMO field campaign is investigated based on an analysis of high-resolution global ocean general circulation model (OGCM) simulations. These MJO events generated exceptionally strong local ocean response that lasted more than one month.

The simulation of the ITF is still a major challenge for ocean and climate models because it is a part of the global ocean circulation, and the complex bathymetry and topography in the Indonesian seas must be adequately resolved. Such studies with high-resolution global OGCMs have been reported in recent years (e.g., Metzger et al. 2010; Shinoda et al. 2012). For example, Metzger et al. (2010) used a 1/12° grid global ocean model, the Hybrid Coordinate Ocean Model (HYCOM), and demonstrated that the model is able to reasonably simulate the ITF transport in major straits in the Indonesian seas and its seasonal variations. In this study, we will use the same global model in which the horizontal resolution is further increased to 1/25° to study the impacts of the unique convection events associated with the strong MJO during CINDY/DYNAMO field campaign on ITF. The finer model grid significantly improves the realism of the complex topography in the Indonesian seas over earlier HYCOM runs (Hurlburt et al. 2011).

Since most previous studies that discuss the Kelvin wave influence on the ITF focus on sea surface height (SSH) fields, particular emphasis in this study is given to the large-scale upper-ocean velocity variability associated with Kelvin wave propagation that influences the ITF transport.

2. Model and experiments

The model used in this study is the global HYCOM. Since details of the model physics and numerical schemes are reported in other papers (e.g., Bleck 2002; Chassignet et al. 2003), here, we describe only the aspects that are relevant to our study. HYCOM is a community ocean model with a generalized vertical coordinate (Bleck 2002). The *K*-profile parameterization (KPP; Large et al. 1994) is used for vertical mixing in the model. The model domain is global, and it has a very high horizontal resolution (1/25°, 4.4 km at the equator), which can adequately resolve the small islands and narrow straits in the Indonesian seas. It includes 41 layers in the vertical with enhanced resolution in the upper 100 m. The model topography datasets were derived from 30-arc-s General Bathymetric Chart of the Oceans (GEBCO) with substantial hand editing based on a combination of navigational charts and scientific

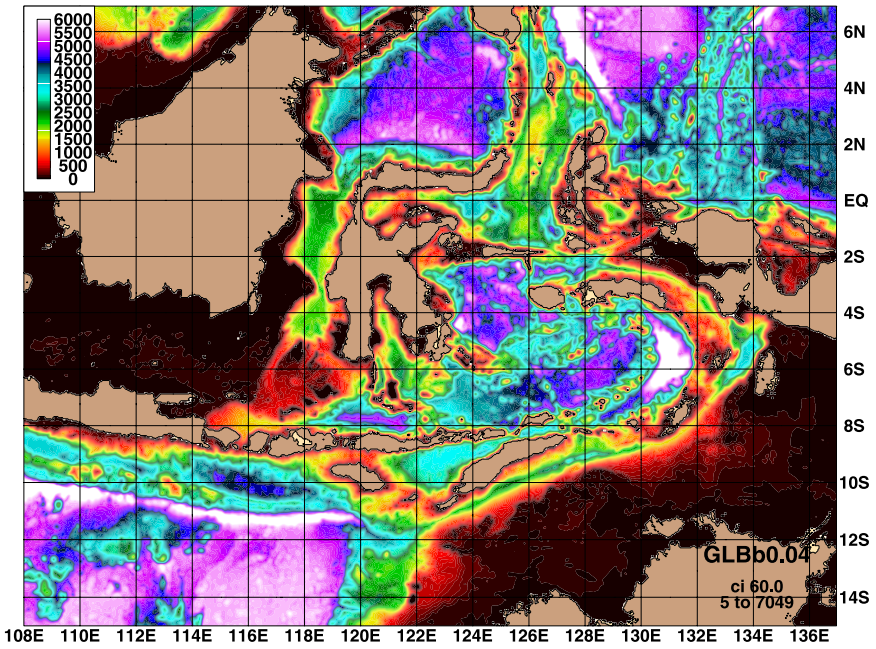

FIG. 1. The 1/25° grid global HYCOM topography (m) for the subregion of the Indonesian seas.

literature, similar to what was described in Metzger et al. (2010). The model topography around the Indonesian seas is shown in Fig. 1.

The global HYCOM simulation was spun up for 10 years with daily climatological atmospheric forcing fields derived from ERA-40 (Kållberg et al. 2004) after initializing from the Generalized Digital Environmental Model, version 4 (GDEM4), hydrographic climatology (Carnes et al. 2010). The model was then integrated for the period 2008–12 with archived operational forcing from the Navy Operational Global Atmospheric Prediction System (NOGAPS; Rosmond et al. 2002) but with the long-term annual mean replaced by the long-term mean from ERA-40. The wind speed was corrected using a monthly climatology from QuikSCAT (Kara et al. 2009). Observational data are not assimilated in this simulation. It should be noted that the 1/25° grid HYCOM is the highest resolution so far for the global ocean model study that investigates ITF variability.

3. Observational data for the model evaluation

a. DYNAMO and RAMA buoy data

In situ data collected from a surface mooring during the DYNAMO field campaign (Chi et al. 2014), which is located at 0°, 78°56′E, are used to evaluate upper-ocean variability in the model simulation. A major focus of the evaluation is on upper-ocean currents near the equator generated by strong westerly winds since these currents cause remote ocean variability through oceanic wave propagation, which is the primary subject of this study.

The velocity data at the DYNAMO buoy site are collected from the measurements of an upward-looking 300-kHz acoustic Doppler current profiler (ADCP) at 100-m depth, a 1200-kHz ADCP at 19-m depth, a Doppler volume sampler (DVS) at 8-m depth, a DVS at 3-m depth on the surface moorings, and an upward-looking 75-kHz ADCP at 600-m depth on the subsurface moorings. The vertical resolution of the oceanic current observation is 0.5 m for the DVS and 1200-kHz ADCP, 2 m for the 300-kHz ADCP, and 8 m for the 75-kHz ADCP. The velocity datasets on a 2-m vertical interval were created using these DYNAMO buoy measurements and are used to evaluate the model simulation.

Although the equatorial DYNAMO buoy measured meteorological variables, the sensors were vandalized on 20 November 2011 before the onset of the strong MJO event in late November. Since near-surface winds measured by Research Moored Array for African–Asian–Australian Monsoon Analysis and Prediction (RAMA; McPhaden et al. 2009) buoy located nearby the DYNAMO buoy (0°, 80.5°E) are available for the period of DYNAMO including late November and December after the onset of the strong MJO event, they are used to evaluate the surface wind fields that are used to force the model. The winds at 4 m above the sea surface are measured every 10 min, and the daily mean of these data are compared with the model forcing fields.

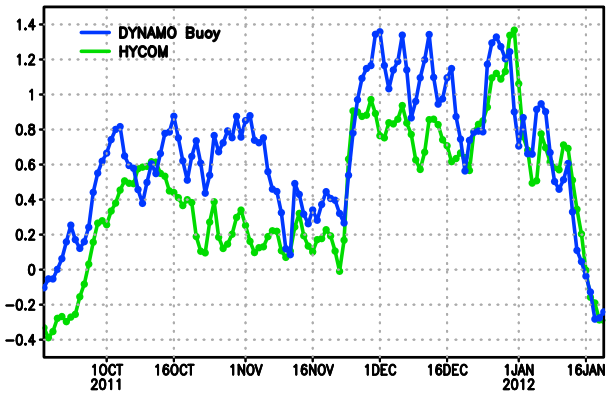

FIG. 2. Time series of daily mean surface zonal velocity (m s^{-1}) from the DYNAMO mooring at 0°, 79°E (blue line) and from 1/25° grid global HYCOM (green line).

b. *Satellite observations*

The SSH data obtained from Archiving, Validation, and Interpretation of Satellite Oceanographic Data (AVISO) are also used to evaluate local and remote ocean response in the model simulations. We use the daily SSH data on 0.25° × 0.25° grid derived from multisatellite analyses. Data derived from multiscale ultrahigh-resolution (MUR) sea surface temperature (SST) analysis are used to compare with SST variability from the model simulations within the Indonesian seas. The data are created by the combined analysis derived from both microwave and infrared sensors on satellites. The SST data are presented in the form of daily average SST fields on a 0.011° × 0.011° grid. Daily SST data on a 0.25° × 0.25° grid from the blended product of satellite and in situ observations (Reynolds et al. 2007) are also used for the comparison. Near-surface velocity data, derived from the Ocean Surface Currents Analyses–Real Time (OSCAR) project (Lagerloef et al. 1999), are used to compare the spatial pattern of surface currents of the model simulation. The OSCAR velocities are presented in the form of 5-day average near-surface velocity fields on a 1° × 1° grid. In addition to winds from NOGAPS that are used to force the model, surface wind data from WindSat measurements (Gaiser et al. 2004) are used to compare the wind fields during DYNAMO with those in other MJO events. We use 3-day average 10-m-height winds on a 0.25° × 0.25° grid.

4. Results

a. *Comparison of the model simulations with observations*

The variability of surface and subsurface currents in the model simulation is first compared with the observed data. Figure 2 shows the time series of observed and

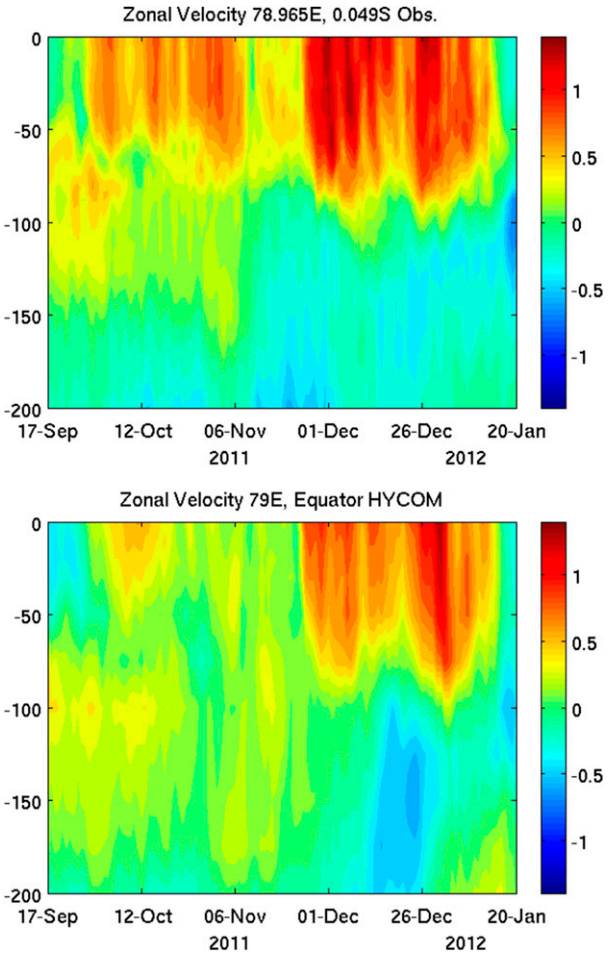

FIG. 3. Time–depth cross sections of zonal velocity (m s^{-1}) at 0°, 79°E (top) from the DYNAMO mooring and (bottom) from the 1/25° grid global HYCOM.

modeled surface zonal current from mid-September 2011 to mid-January 2012 at the DYNAMO surface mooring location. The model surface current represents the average current in the upper 5 m. Variations of zonal currents simulated by the model agree with observations

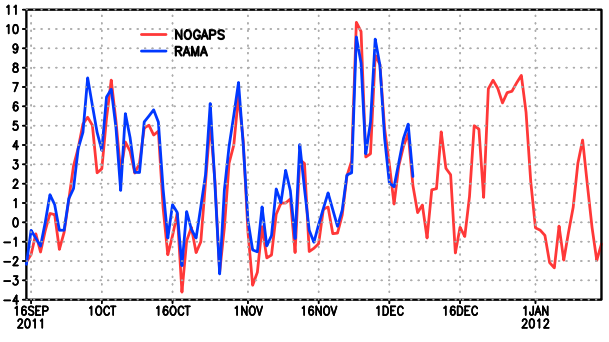

FIG. 4. Time series of daily mean zonal winds (m s^{-1}) at 10-m height at 0°, 80.5°E from the RAMA mooring (blue line) and NOGAPS (red line).

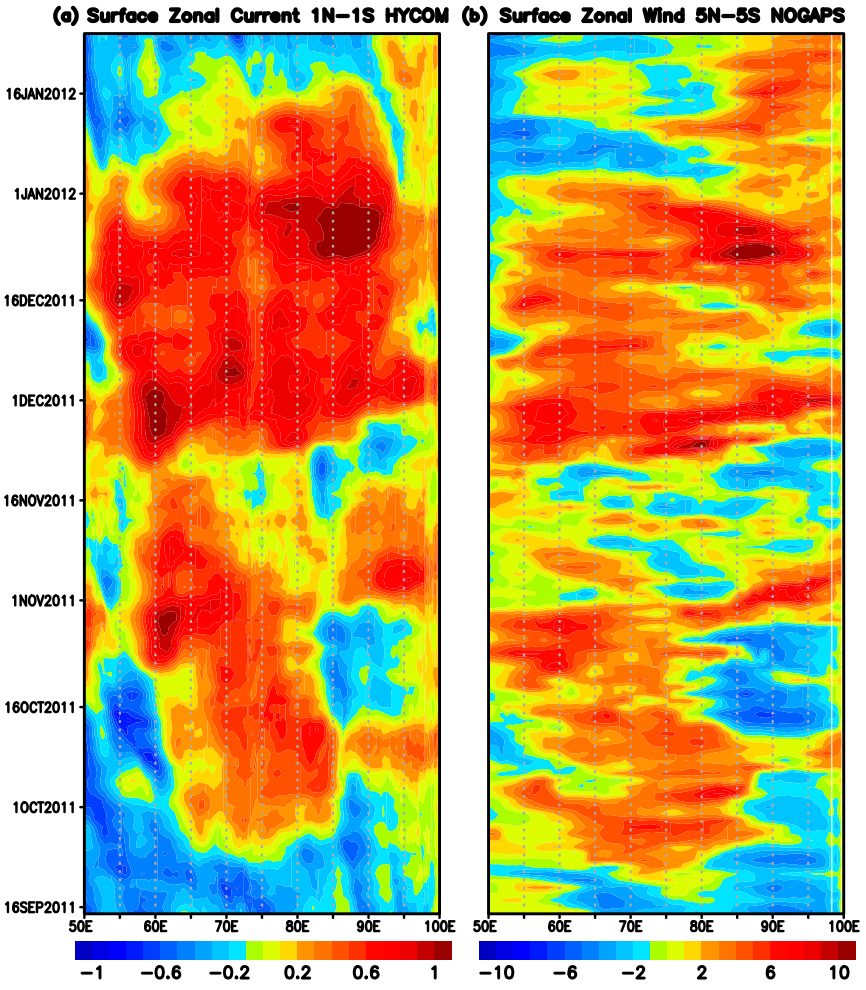

FIG. 5. (a) Longitude–time diagram of surface zonal velocity ($m\,s^{-1}$) averaged between 1°N and 1°S from the $^{1}/_{25}$° grid global HYCOM simulation. (b) Longitude–time diagram of zonal wind ($m\,s^{-1}$) at 10-m height averaged between 5°N and 5°S.

reasonably well. In particular, the acceleration of equatorial jet in late November and late December is well simulated by the model. Additionally, the rapid decrease of zonal current from the end of December to mid-January in the model agrees very well with observations. However, there are some discrepancies between the model and observations. For example, the strong equatorial jet in the model during early December is underestimated. While the observed jet is about 0.9–1.4 $m\,s^{-1}$, the jet simulated by the model is 0.8–1 $m\,s^{-1}$. This could be partly due to the weaker eastward current in the model before the acceleration in late November. There are large fluctuations of the zonal current with a magnitude of approximately 0.4 $m\,s^{-1}$ and period of around 5–7 days during early December in observations. Similar fluctuations are evident in the model, but their magnitude is smaller (~0.2 $m\,s^{-1}$). A relatively strong fall Wyrtki jet (Wyrtki 1973) of 0.4–0.8 $m\,s^{-1}$ is observed from October to early November. Although the Wyrtki jet is also evident in the model, it is weaker than the observation by about 0.2–0.4 $m\,s^{-1}$.

It should be noted that the DYNAMO and RAMA moorings are located in an area of large zonal gradients of the zonal velocity associated with the Wyrtki jet (section 4b), and thus model–data comparisons at specific locations around this area can easily show large discrepancies. Another possible reason for the underestimation of eastward zonal currents is errors in the upper-ocean stratification of HYCOM. The main thermocline in HYCOM is deeper by about 20 m than observations (not shown). The locally driven zonal jet could be weaker because of the thicker upper layer. However, a deeper thermocline in the model is also evident after the strong westerlies in late November, and

thus discrepancies between the model and observations are not fully explained by the upper-ocean stratification.

Figure 3 displays the vertical structure of zonal current on the equator for the same period as in Fig. 2. The vertical extent of the equatorial jet simulated by HYCOM agrees well with observations. The eastward jet extends to the depth of about 80–90 m in late November–December. There are weak westward currents below the strong eastward jet in the observations, which is located around 100–200 m and is successfully simulated by the model, albeit with somewhat stronger magnitude in early December. Upward propagation of the westward current is clear in both observations and model.

The zonal winds at 10-m height from NOGAPS, which are used to force the model, are compared with those from the RAMA buoy measurement at 0°, 80.5°E (Fig. 4). Zonal winds at 4 m measured by the RAMA buoy are extrapolated to 10 m using air temperature, humidity at 2 m, and SST with the TOGA COARE bulk flux algorithm (Fairall et al. 1996, 2003). The zonal winds from NOGAPS agree very well with RAMA observations. In particular, the timing and strength of strong westerly winds during the MJO onset in late November are quite similar. The two peaks of westerly winds with the strength of 9–10 m s^{-1} during this period are associated with the convectively coupled Kelvin waves with heavy precipitation events (e.g., Moum et al. 2013).

While the zonal winds from NOGAPS and RAMA buoy are also similar before the strong wind event (September–mid-November), there are some quantitative differences. During this period, NOGAPS winds often underestimate the westerlies and overestimate the easterlies, which could be partly responsible for the weaker Wyrtki jet simulated by the model for this period. The discrepancies of the observed and simulated zonal currents, however, are much more apparent than those in forcing fields, and thus they cannot be entirely attributed to the errors in the local forcing fields. Since remotely forced equatorial waves and equatorial resonance may contribute to the generation and maintenance of Wyrtki jets (e.g., Jensen 1993; Han et al. 1999; Qiu et al. 2009; Nagura and McPhaden 2010), the errors in the zonal current during this period could be due to the errors in winds in other regions as well as errors resulting from the model deficiencies.

Although there are some notable differences of surface and subsurface currents between the model and observations shown in Figs. 2 and 3, the model reproduces the time evolution of zonal current reasonably well. In particular, the generation of the long-lasting strong equatorial jet during late November–December and the subsequent rapid decay during January are both well simulated by the model. Consequently, the model can be used to examine the relevant dynamical processes associated with remote and local ocean responses during the period of DYNAMO observations.

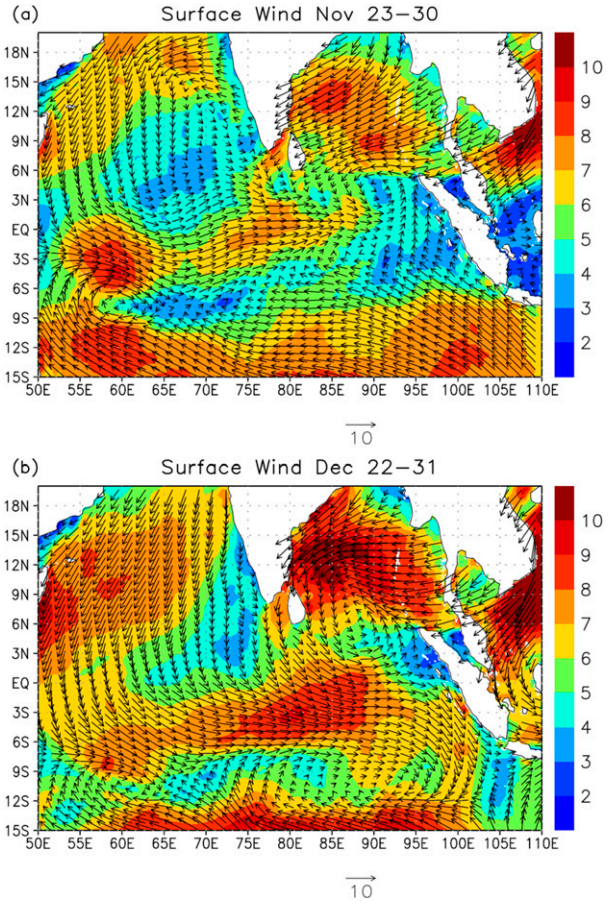

FIG. 6. (a) Average winds (m s^{-1}) at 10 m (vectors) and wind speed (shading) from NOGAPS during 23–30 November 2011. (b) As in (a), but the period 22–31 December 2011. The reference vector is plotted below each panel.

b. *Large-scale variability of the equatorial zonal jet*

In this section, large-scale upper-ocean variability in response to the MJO events in the model is described and compared with the satellite-derived data. Figure 5a shows the longitude–time diagram of surface zonal current near the equator from the HYCOM simulation. The rapid acceleration of the equatorial jet in late November occurs across almost the entire Indian Ocean Basin. The large-scale eastward currents continue to be strong until early January. While the strong currents that exceed 1 m s^{-1} are found in both the western and eastern parts of the basin during late November–early December, they prevail only in the eastern basin around 80°–90°E in late December. This distribution of zonal current is consistent

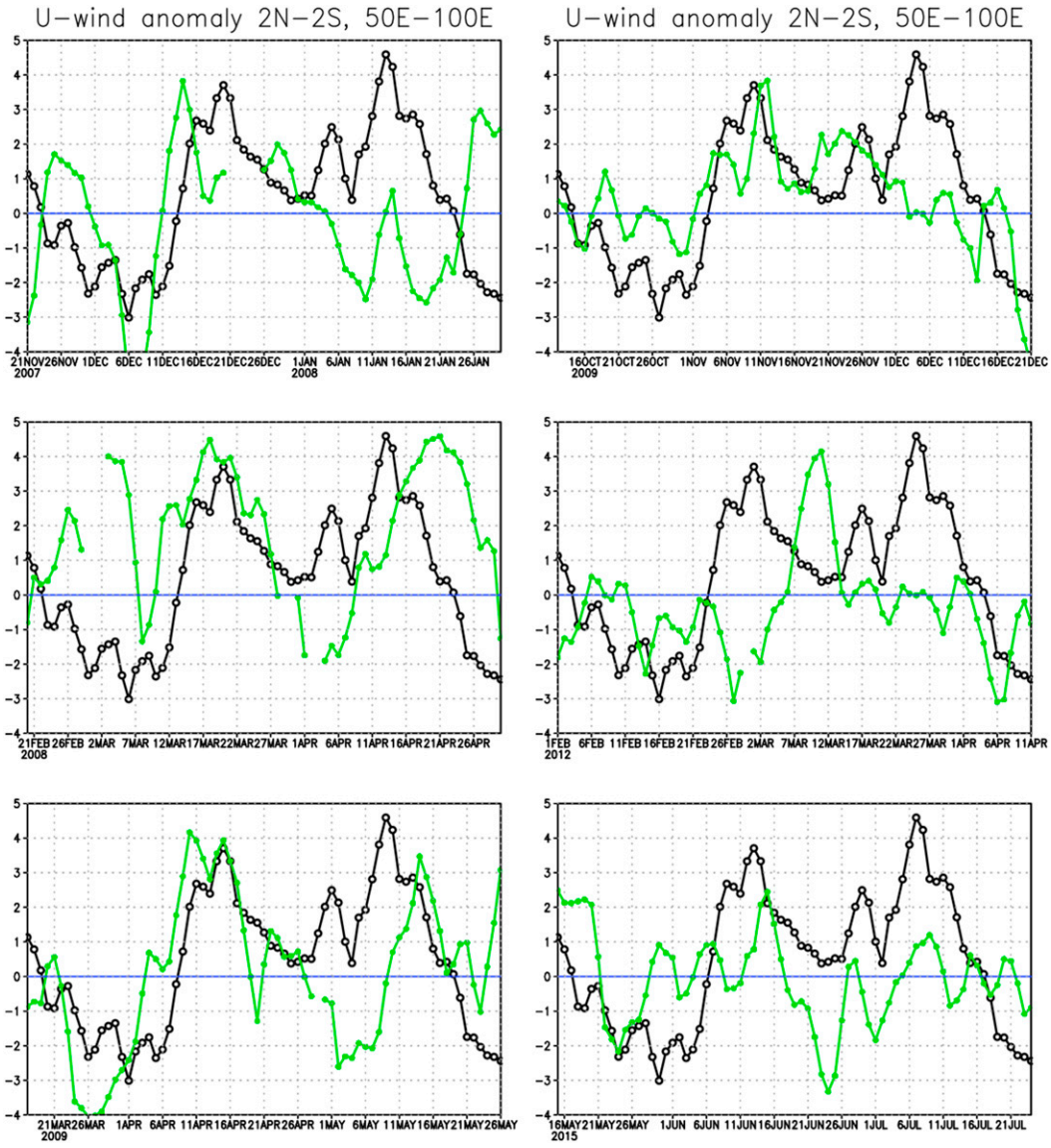

FIG. 7. Time series of zonal wind anomaly ($m\,s^{-1}$) at 10 m averaged over the area 2°N–2°S, 50°–100°E derived from WindSat measurements. Black lines in all panels indicate the time series for the period 1 November 2011–10 January 2012. The periods of time series shown by green lines are indicated in the horizontal *x*-axis labels when strong MJO events were observed.

with the spatial pattern of westerly winds, with strong westerlies being confined to the eastern Indian Ocean in late December (Figs. 5b and 6). During late November, equatorial westerlies are found almost in the entire equatorial basin, and they are stronger in the western basin. The strong westerly winds in late December are associated with the large-scale cyclonic circulation centered around 6°N, 90°E in the Bay of Bengal (Fig. 6). The spatial pattern of NOGAPS surface winds during these periods is consistent with those from satellite observations (Shinoda et al. 2013b). It should be noted that strong zonal winds are centered near the equator, where the ocean response is strongest, during these events.

A significant zonal (spatial) variation in the strength of the equatorial jet (e.g., early December) is found in the entire basin, including the location of the DYNAMO mooring. For example, during early December, the surface zonal current varies spatially by about 0.2–0.4 $m\,s^{-1}$ around 80°E. Hence, it is not surprising if the comparison between the model and observations at a single location shows notable

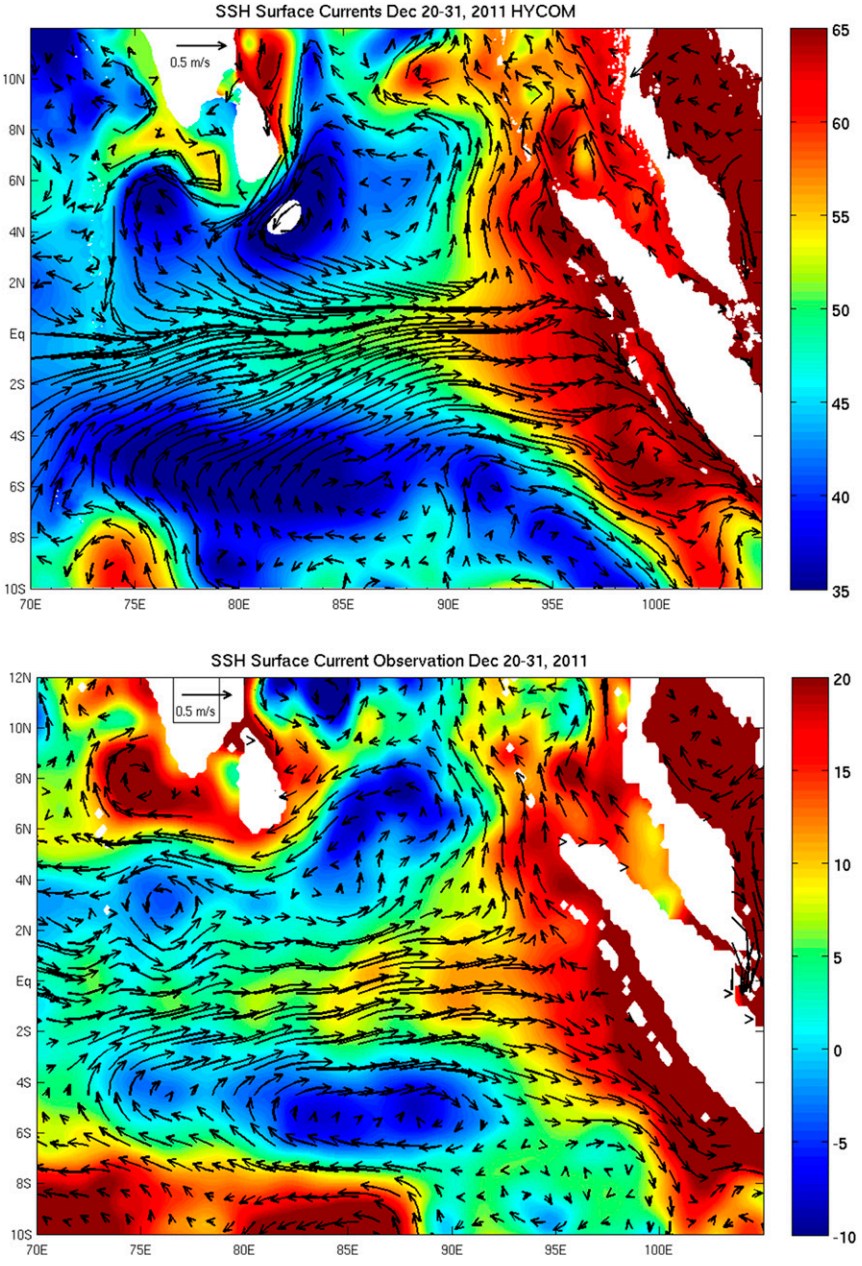

FIG. 8. (top) Surface velocity ($m\,s^{-1}$) and SSH (cm) during 20–31 December from HYCOM. (bottom) Surface velocity ($m\,s^{-1}$) from OSCAR and SSH (cm) from satellite altimeter data during 20–31 December. The total range of the color bar in the two panels is 30 cm, but the SSH values of each color are different for each panel.

discrepancies since the model may not be able to accurately simulate details of mesoscale features.

The westward propagation of zonal surface current during October–early November is clearly evident (Fig. 5a), which is consistent with previous observational studies (e.g., Molinari et al. 1990; Qiu et al. 2009; Nagura and McPhaden 2010). During this time, the Wyrtki jet is mostly found in the central and western basin, and it can be clearly distinguished from the strong equatorial jets that are generated by westerlies associated with the MJO in late November and December (e.g., Jensen et al. 2015). Again, it should be noted that the strong zonal gradient of zonal velocity associated with the Wyrtki jet is located in the central Indian Ocean near the DYNAMO and RAMA moorings. For example, in mid- to late October, eastward currents of about $0.5\,m\,s^{-1}$ are found

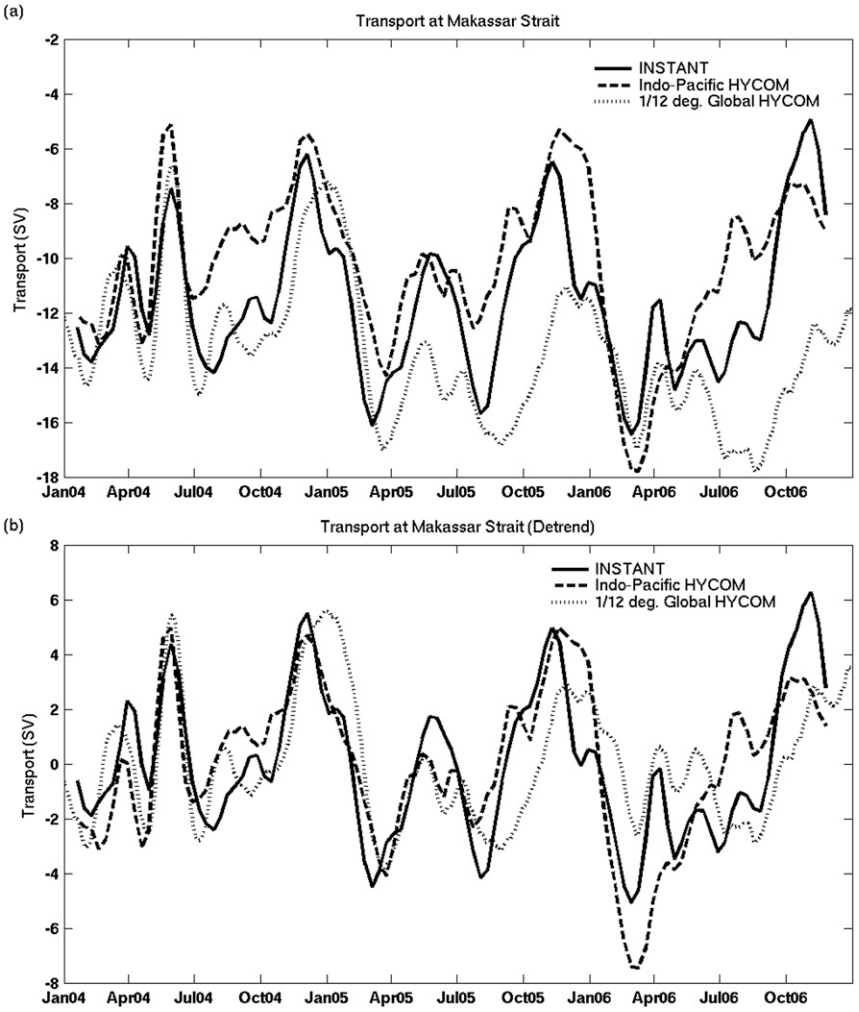

FIG. 9. (a) Total southward transport (Sv) at the Makassar Strait during 2004–06 from the INSTANT moorings (solid line), Indo-Pacific basin HYCOM (dashed line), and $^1/_{12}°$ grid global HYCOM (dotted line). Negative transport is southward. A 30-day running filter has been applied to all time series. Adopted from Shinoda et al. (2012). (b) As in (a), but the linear trends are removed and the means are subtracted.

around 80°E while the westward currents are evident around 84°E. Even a slight error in simulating the location of the large zonal gradient can cause significant discrepancies when comparing observation and model at a single location during this period. Thus, the notable difference of Wyrtki jet strength between the model and observations shown in Fig. 3 could be caused by even a very small error of surface forcing fields. Note also that the large zonal gradient is found in the zonal winds near the equator during this period (Fig. 5b).

Strong jets, which are comparable to those observed during DYNAMO, have been observed in the equatorial Indian Ocean in response to other MJO events (e.g., Shinoda et al. 2013a). However, it should be emphasized here that the zonal jet remained strong in the entire Indian Ocean Basin lasting more than one month during DYNAMO, which is unlike other events. This is because the MJO events in late November and December, which are both associated with strong westerlies, occurred within one month without a clear suppressed phase between them, and the period of weak zonal winds being observed in mid-December was very short (Fig. 5b). Such long duration of large-scale strong zonal jets in response to the MJO is unusual in this region.

To further demonstrate that these surface wind fields during this period are indeed unique, the time series of equatorial surface winds during DYNAMO are compared with those associated with other strong MJO events in recent years (Fig. 7). Surface winds are derived from WindSat measurements for the period 2004–15.

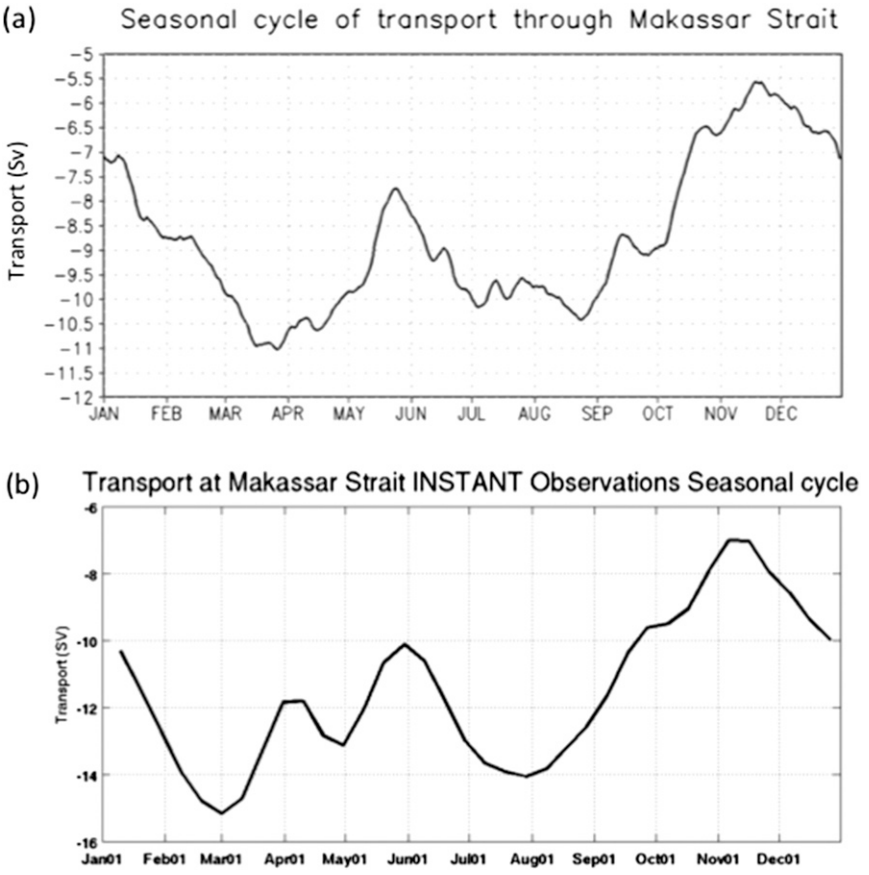

FIG. 10. (a) Seasonal cycle of the transport through the Makassar Strait at the INSTANT mooring location derived from the 28-yr simulation of the Indo-Pacific basin HYCOM (adopted from Shinoda et al. 2012). (b) Seasonal cycle of the transport through the Makassar Strait from the INSTANT observations.

Strong MJO events are selected based on the index defined by Wheeler and Hendon (2004). The time series during DYNAMO show that large-scale westerly anomalies lasted about 40 days from late November 2011 to early January 2012. Such long duration of westerly anomaly is not found in other MJO events, although some of the events are associated with westerly anomalies as strong as those during DYNAMO. Consequently, large-scale strong eastward jets with long duration are generated because of the occurrence of two strong events in a short time period.

As a result of the strong equatorial jet and the convergence at the eastern boundary in late November–December, a significant increase of SSH (~20 cm) is found in the large areas (6°N–8°S) near the coast (Fig. 8, top). The alongshore (northwesterly) winds south of the equator in late December (Fig. 6) could further enhance the SSH increase. A similar SSH anomaly increase is evident in satellite altimeter observations (Fig. 8, bottom). Also, the spatial pattern of equatorial and off-equatorial surface currents simulated by the model is consistent with that derived from OSCAR analysis, but the equatorial jet in the model is stronger (Fig. 8). This could be partly due to the underestimation of the equatorial jet in OSCAR during this period (Shinoda et al. 2013b).

c. *Variation of Indonesian Throughflow*

1) SEASONAL VARIATION

During the International Nusantara Stratification and Transport (INSTANT) program (Sprintall et al. 2004, 2009; Gordon et al. 2008), a prominent seasonal variation of the Indonesian Throughflow was observed. The solid line in Fig. 9a shows the ITF transport estimate based on the mooring observations at the Makassar Strait, which is the primary passage of the ITF, carrying about 80% of its total transport (Gordon 2005). The semiannual variation of ITF transport is apparent. There are significant reductions of southward currents at the Makassar Strait during April–May and October–November

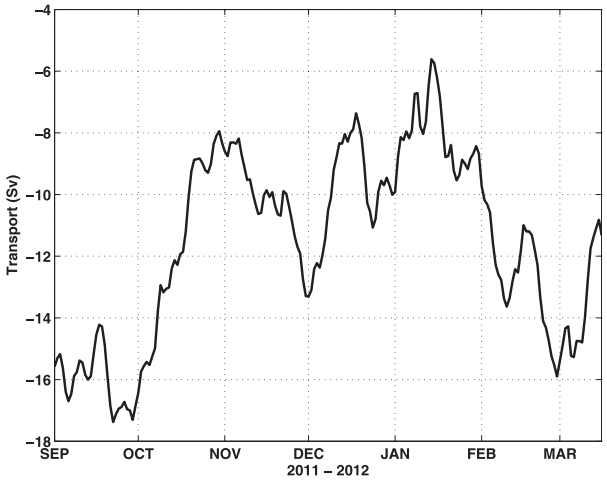

FIG. 11. The total transport (Sv) through the Makassar Strait at 2.88°S from the 1/25° grid global HYCOM simulation.

and subsequent rapid recovery during December–March (Gordon et al. 2008; Susanto et al. 2012). The semiannual cycle is evident in longer time series (2004–09) of mooring data at the Makassar Strait (Susanto et al. 2012) and proxy time series using satellite-derived SSH data (Susanto and Song 2015).

Figure 9 also includes the ITF transport at the Makassar Strait simulated by the high-resolution (1/12°) global HYCOM (Shinoda et al. 2012), which is essentially the same model as the one used in this study except for the horizontal resolution. While there are significant differences in the mean transport (Fig. 9a), the model is able to simulate the variation well, including the semiannual cycle (Fig. 9b). Furthermore, the similar seasonal cycle is found in the long-term (28 yr) integration of the Indo-Pacific basin HYCOM (Fig. 10). While the timing and magnitude of the reduction of southward transport during boreal spring somewhat varies each year in observations (Fig. 9), the rapid recovery during December–March of each year is consistent with that in the seasonal cycle from the long-term HYCOM simulation (Fig. 10).

2) VARIATION OF ITF DURING DYNAMO

The total transport through the Makassar Strait during the period of the DYNAMO field campaign from the global HYCOM simulation is shown in Fig. 11. Note that the INSTANT mooring data are not available during the DYNAMO period. A large variation of transport through the Makassar Strait is found. The variations during September–November is consistent with the seasonal cycle

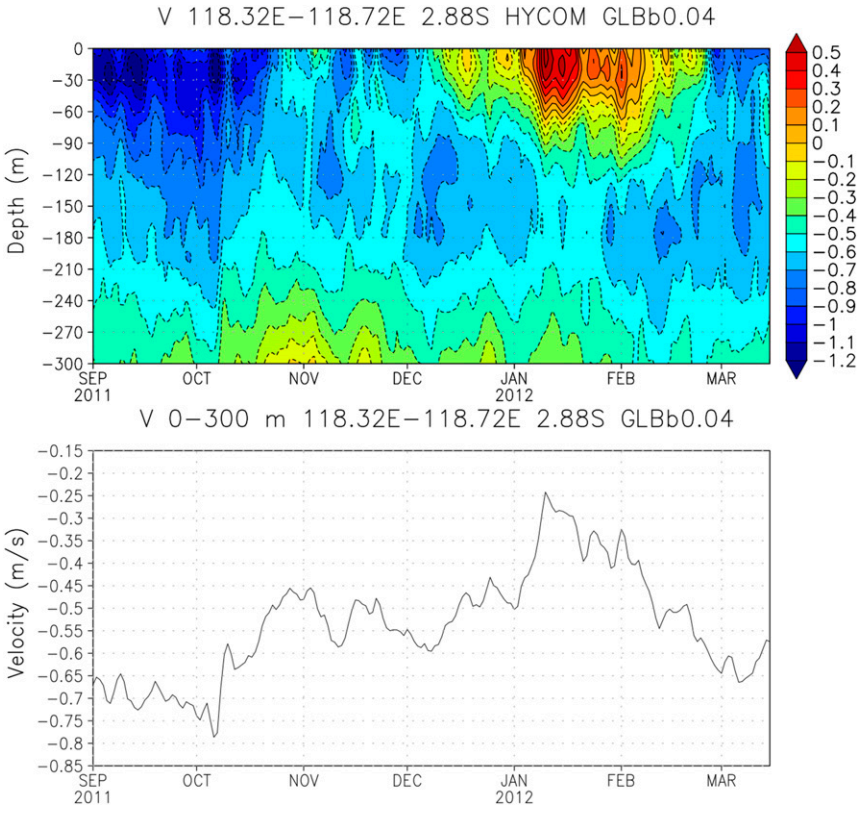

FIG. 12. (top) Meridional velocity (m s^{-1}) at the Makassar Strait, 2.88°S, 118.32°–118.72°E. (bottom) Average meridional velocity in the upper 300 m at 2.88°S, 118.32°–118.72°E.

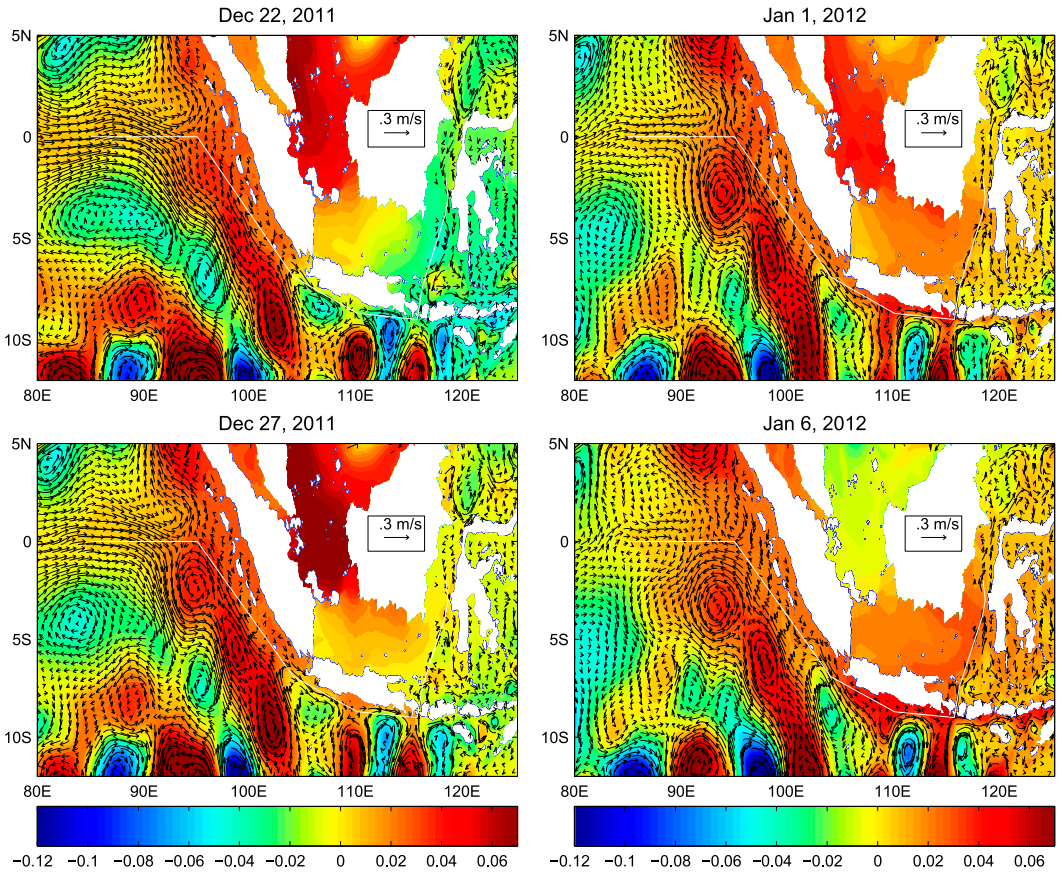

FIG. 13. SSH (shading; m) and upper-ocean (average over 0–150-m depths) velocity (vectors) anomalies during 22 and 27 December 2011 and 1 and 6 January 2012 relative to the mean of December 2011–January 2012 from the HYCOM simulation. A 30-day running filter has been applied to the time series. The reference vector is shown over Kalimantan.

in which the strong southward transport in September is reduced by early November. After mid-December–early January the transport continues to be small and is further reduced by mid-January, in contrast to the seasonal cycle in which the large southward transport starts recovering rapidly from mid-December. The minimum southward transport during mid-January is less than 6 Sv, which is considered to be a large deviation from the seasonal cycle (Susanto et al. 2012).

The reduction of the transport during this period is mostly due to strong anomalous meridional currents. The along-channel velocity at the INSTANT mooring locations in the Makassar Strait during the period of the DYNAMO field campaign from the global HYCOM simulation is shown in Fig. 12 (top). A large variation of upper-ocean currents through the Makassar Strait is found, especially after the MJO events in November and December (Fig. 12, top). In particular, relatively strong northward currents, which exceed 0.3 m s^{-1}, are found in the upper 100 m in January, and these northward currents lasted more than one month, in contrast to the seasonal cycle in which the rapid recovery of the southward flow occurs from December (Fig. 10). From early to mid-January, the maximum northward velocity exceeds 0.5 m s^{-1}, which is unusual during this season (e.g., Susanto et al. 2012). The variations during September–November are consistent with the seasonal cycle in which the strong southward current in September is reduced in magnitude by early November.

While the average along-channel velocity in the upper 300 m is southward (Fig. 12, bottom), its variation is similar to the currents in the upper 100 m, and a prominent reduction of southward velocity is found during January. The strong northward currents in the upper 100 m largely contribute to this reduction. The variations of upper-300-m along-channel velocity during September–November are consistent with the seasonal cycle in which the strong southward current in September is reduced by early November. However, the large reduction during January is not found in the seasonal cycle in the long-term integration of Indo-Pacific HYCOM and INSTANT observations (Figs. 9 and 10). These variations of the average along-channel velocity in the upper 300 m are similar to the total transport, indicating that the anomalous transport during this period is primarily caused by variations in the upper ocean. Note that the

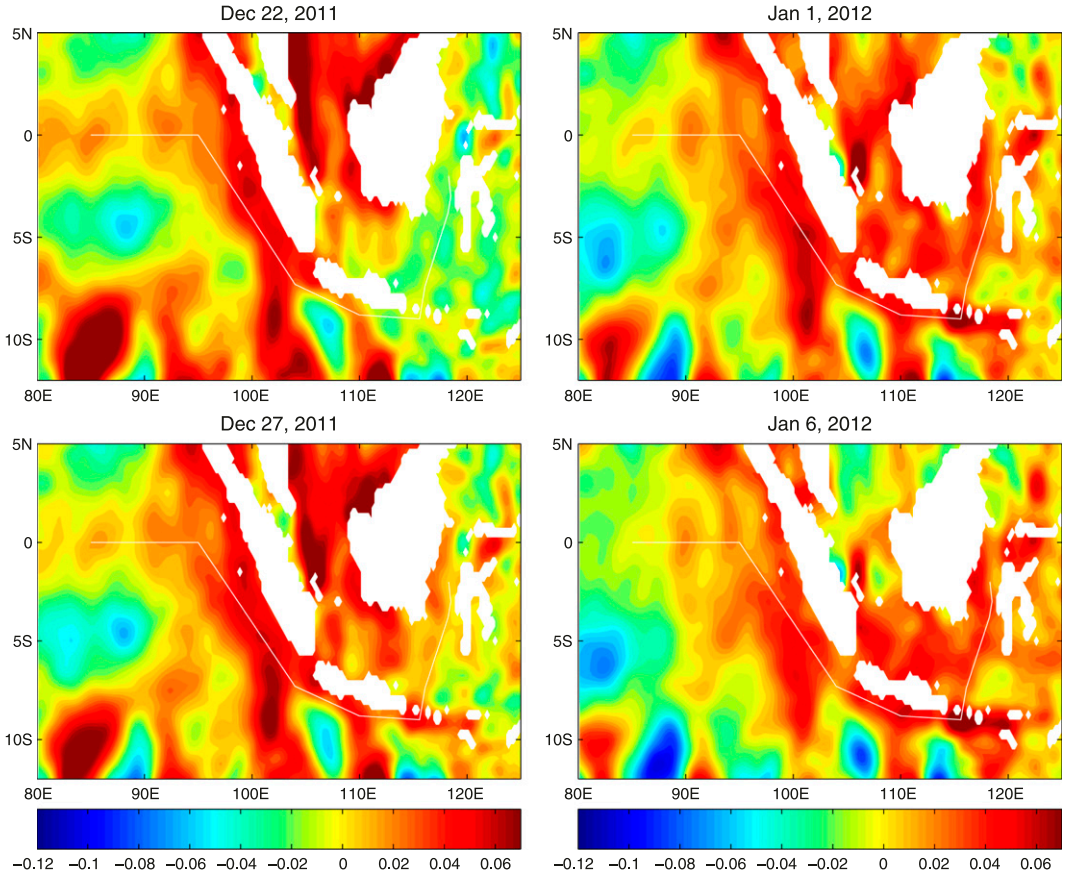

FIG. 14. As in Fig. 13, but only SSH anomalies from satellite altimeter data.

differences in variation between Figs. 11 and 12 are mostly due to differences in the velocity below 300-m depth since significant transport variations could be caused by small changes of velocity in the deeper layer.

These results suggest a substantial impact of MJO on the ITF through the Makassar Strait during this period since the seasonal cycle reveals the rapid recovery of southward transport in December–January (Figs. 9 and 10). The analysis in the following section will demonstrate that these upper-ocean variations during December–February are caused primarily by the remote ocean response to the MJO events observed during DYNAMO, although Ekman transport driven by local winds also contributes.

d. Propagation of Kelvin waves

Figure 13 shows maps of SSH and surface velocity anomalies during mid-December–early January. The anomalies are calculated as those relative to the mean of December–January since the integration period is not long enough to obtain the accurate annual cycle. Even though mesoscale eddies exist off the Java coasts, the propagation of SSH anomalies and alongshore velocity along the coasts of Sumatra and Java is apparent. During mid-December, eastward equatorial jets develop in the central and eastern Indian Ocean, which are associated with the increase in SSH near the eastern boundary. SSH anomalies continue to increase at the eastern boundary and propagate along the coasts of Sumatra and Java during late December–early January (maps of 27 December, 1 January, and 6 January). These high SSH anomalies near the coast are associated with an alongshore (eastward) velocity near the Lombok Strait (8°S, 115°E). A significant portion of the current and SSH anomalies propagate northward through the Lombok Strait in early January and generate anomalous northward currents in the Makassar Strait, although some of the signals propagate eastward across the Lombok Strait. It takes approximately a fortnight for the anomalies associated with the eastward equatorial current to propagate from the eastern boundary near the equator to the Makassar Strait, consistent with the phase speed of a Kelvin wave in this region (e.g., Sprintall et al. 2000). A similar propagation of Kelvin waves along the coast is also evident in satellite altimeter data (Fig. 14). The magnitude of SSH anomalies in mesoscale eddies south of 6°S in the altimeter data is comparable to those found in the model, suggesting that the non-data-assimilative model is able to generate realistic

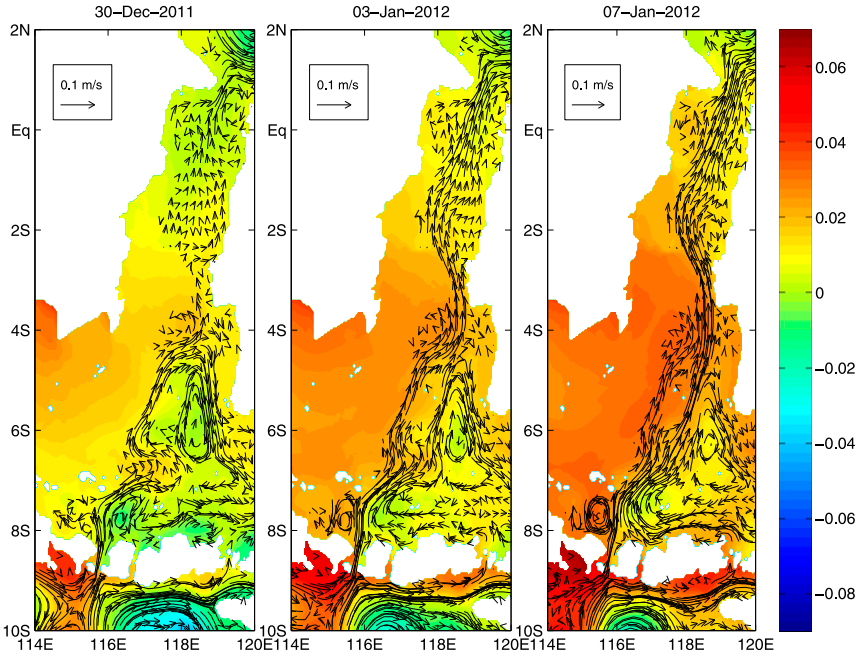

FIG. 15. As in Fig. 13, but for a smaller domain and the periods 31 December 2011 and 3 and 7 January 2012. The reference vector is shown in the top left.

eddies in this region during December–January. While SSH variability associated with the Kelvin wave propagation simulated by the model agrees well with altimeter data, there are some quantitative differences within the Indonesian seas. It should be noted that the accuracy of altimeter data within the Indonesian seas is still somewhat uncertain, and thus the error in the altimeter data might contribute partly to these differences.

The development of a northward current anomaly near the Makassar Strait in early January is further demonstrated in the SSH and current anomaly map for a smaller subregion (Fig. 15). Large positive SSH anomalies near the Lombok Strait are found on 30 December. As the SSH anomalies increase during this period, strong anomalous northward currents in the Lombok Strait are generated. Subsequently, these currents extend farther northward and on 7 January strong anomalous currents are evident in the Makassar Strait. Significant eddy activity is found within the Indonesian seas, which could disturb the signals of propagation; however, the northward propagation is clearly detected in the model.

The propagation of coastal Kelvin waves and their impact on the ITF are clearly and explicitly demonstrated in the velocity and SSH fields along the path of the Kelvin wave. Figure 16 shows the evolution of the alongshore velocity and SSH along the equator in the eastern Indian Ocean, the coasts of Sumatra and Java, and from the Lombok Strait to the Makassar Strait (the white solid line shown in Figs. 13 and 14). Propagation of SSH and velocity anomalies along the coastline and through the Lombok and Makassar Straits is evident. The propagation speed is consistent with the phase velocity of the first-baroclinic-mode free Kelvin wave over the Indian Ocean, which is about 2.5 m s^{-1} (e.g., Moore and McCreary 1990; Han 2005). It should be noted that the observed propagation speed may deviate from the free Kelvin wave speed because of local wind forcing (e.g., Shinoda et al. 2008) and complex bathymetry and topography, such as a shallow shelf along the coast, which are well resolved in the model.

While the propagation of Kelvin waves is shown in both SSH and surface currents, the phase relationship between SSH and the alongshore velocity deviates from the first-baroclinic-mode coastal Kelvin wave solution of the linear shallow water equation. While SSH and alongshore velocity are in phase in the linear wave solution, with the maximum alongshore velocity corresponding to the maximum SSH, the SSH signal in HYCOM often continues to increase after the alongshore velocity reaches its maximum (Fig. 16). A possible reason of this phase lag could be the effect of lateral friction, which acts to reduce the alongshore velocity. At the eastern boundary near the equator, a zonal convergence of currents occurs at the phase of the maximum velocity because of the strong eastward equatorial currents. At the same time, a meridional divergence occurs because of poleward (alongshore) currents that compensate the convergence of zonal equatorial currents. Because of the reduction of divergence due

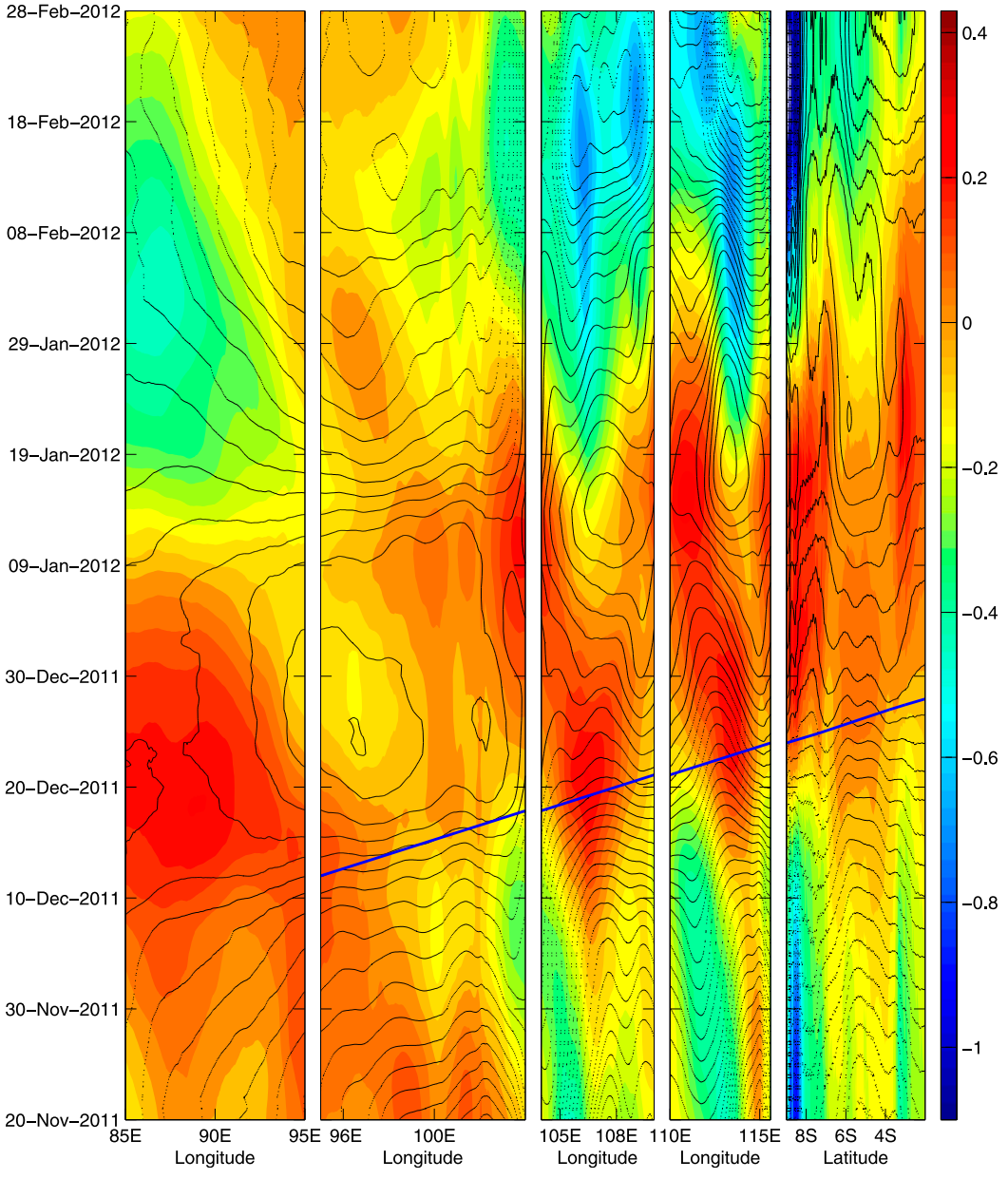

FIG. 16. Alongshore and along-strait velocity (shading; m s^{-1}) and SSH (contour) anomalies along the white solid line shown in Figs. 12 and 13. Both alongshore and along-strait velocities are defined as the velocity component along the white line. Contour interval is 1.0 cm; the dashed contour lines indicate negative values and blue solid lines indicate the phase line of 2.5 m s^{-1}.

to the lateral friction along the coast, SSH could continue to increase after the maximum alongshore velocity. Since lateral friction acts to reduce alongshore velocity, the SSH and velocity fields could deviate from the free Kelvin wave solution and thus contribute to their phase lag.

The surface forcing field also could cause the phase lag between SSH and alongshore velocity. Figure 17 shows the surface wind stress and associated Ekman transport during the Kelvin wave propagation. Northwesterly wind stress along the coast of Sumatra around 3°–6°S generates large Ekman transport toward the coast during 21–25 December when positive anomalous SSH associated with Kelvin waves is evident in this region (Fig. 17a). This alongshore wind stress thus continuously enhances the positive SSH anomaly. During 26–30 December when SSH anomalies extend farther to the coast of Java, significant shoreward transport is found around the coast of Java (Fig. 17b), suggesting that alongshore

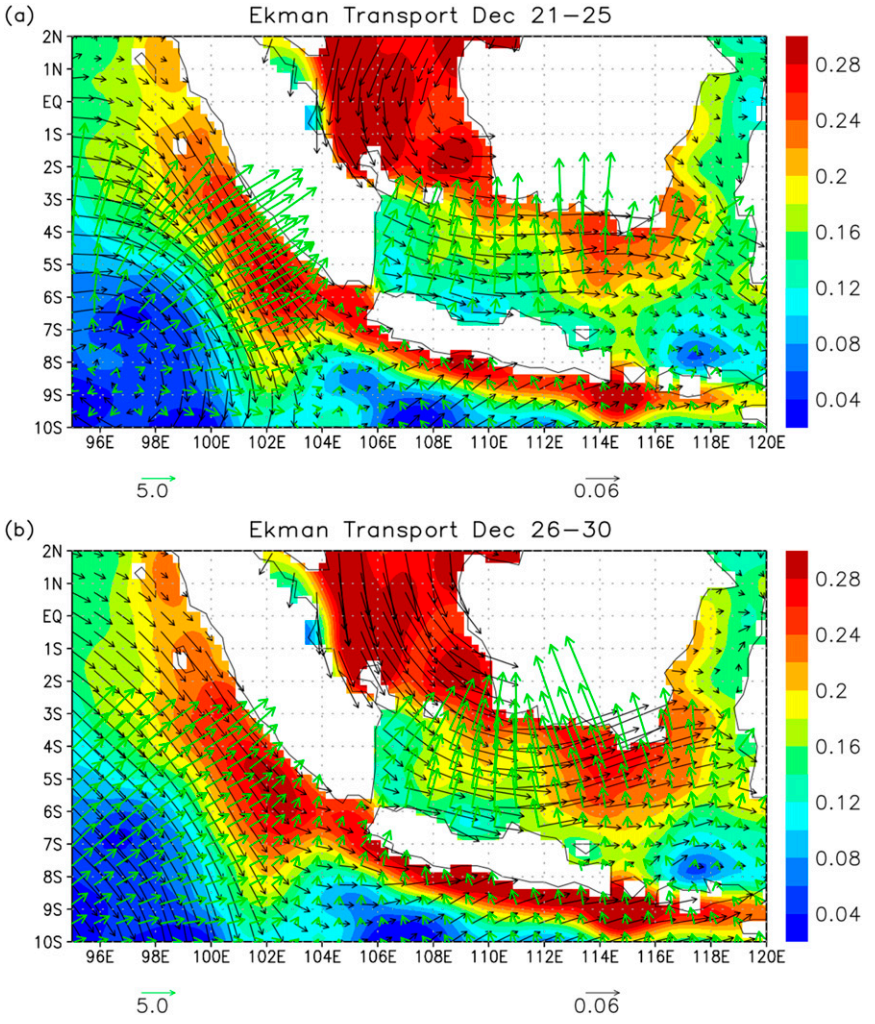

FIG. 17. Ekman transport (green vectors; $m^2 s^{-1}$) and surface wind stress (black vectors; $N m^{-2}$) derived from NOGAPS winds and SSH anomaly (shading; m) from altimeter data during (a) 21–25 December and (b) 26–30 December 2011.

wind stress could effectively influence SSH fields during the Kelvin wave propagation. In addition, alongshore winds may initially drive an alongshore component of currents since it takes significant amount of time to generate steady Ekman currents, especially near the equator. The continuous SSH changes and alongshore component of surface currents directly driven by local winds could contribute to the phase lag.

Previous studies on Kelvin wave propagation and its impact on the ITF mostly focus on SSH variability. However, this study clearly demonstrates the phase lag between SSH and surface velocity, in which the velocity significantly leads the SSH, and thus the velocity fields deduced by SSH from the Kelvin wave solution are often inaccurate. Hence, it is important to describe both velocity and SSH associated with the Kelvin wave propagation to understand the impact of equatorial westerlies on ITF variations.

The strong eddy activity near the coast of Java during the boreal fall–winter season is consistent with previous studies (e.g., Feng and Wijffels 2002; Yu and Potemra 2006; Shinoda et al. 2012). To further demonstrate the interaction with eddies, SSH and velocity anomalies in a smaller subregion near the coast of Java are shown in Fig. 18. Before significant SSH anomalies associated with Kelvin waves reach near the Java coast (17 December), a strong cyclonic eddy centered around 113°E near the coast is found and an anticyclonic eddy centered around 110°E is evident (Fig. 18a). Westward currents associated with the anticyclonic eddy and eastward currents associated with cyclonic eddy are evident near the coast (Fig. 18a). As the Kelvin wave propagates into this region, the anticyclonic eddy moves toward the coast and weakens while the alongshore velocity associated with cyclonic eddy is

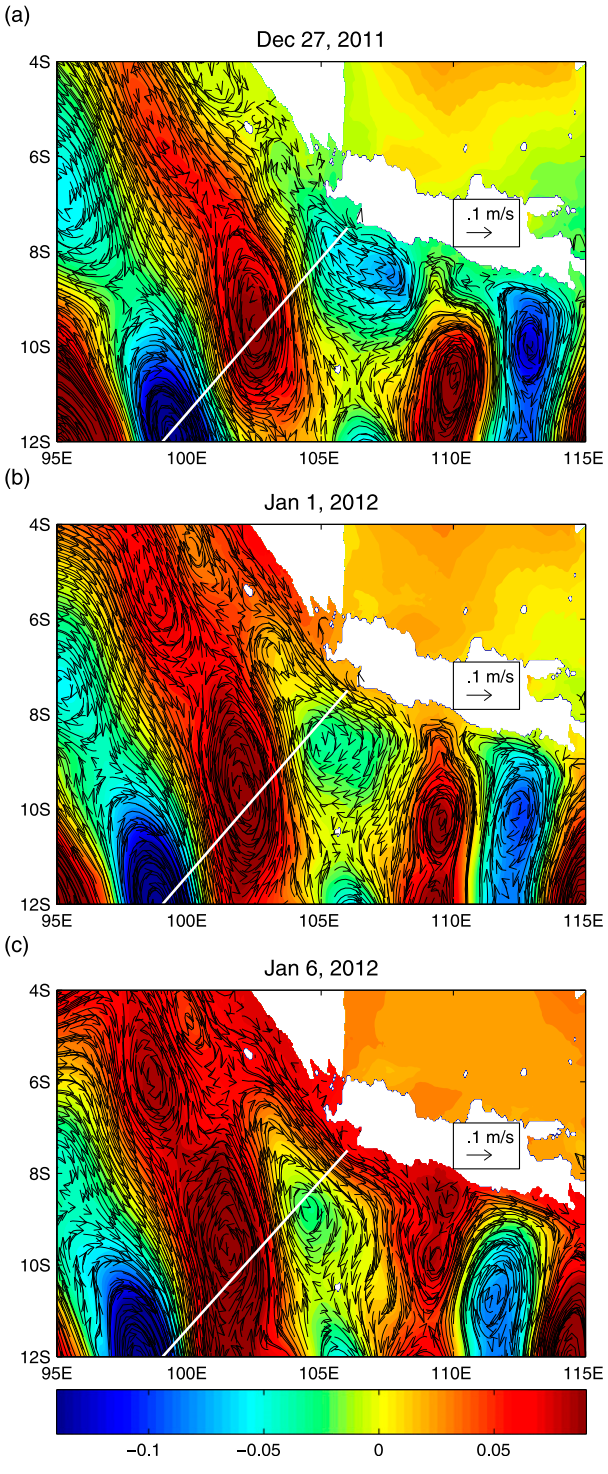

FIG. 18. As in Fig. 13, but for a smaller domain and the periods (a) 27 December 2011 and (b) 1 and (c) 6 January 2012, and a 10-day running mean filter has been applied.

enhanced. The result suggests that the intraseasonal variability of alongshore velocity near the coast is partly caused by the interaction between Kelvin waves and eddies, and these variations could possibly propagate farther along the coast and may impact the circulations in the Indonesian seas including the ITF.

The behavior of these eddies near the coast in the model is consistent with that in the satellite altimeter data. For example, positive SSH anomalies around 10°–12°S, 100°E and negative SSH anomalies around 10°S, 113°E are found in the altimeter data (Fig. 14), and the positive anomalies are connected to those associated with Kelvin wave propagation. Also, positive SSH anomalies (and thus an anticyclonic eddy) centered around 9°S, 100°E are connected to those along the coast of Sumatra (Fig. 14), which is similar to the model result (Fig. 18).

Figure 19 shows the vertical section of alongshore velocity associated with eddies and Kelvin wave propagation. A subsurface maximum of the alongshore (eastward) velocity associated with the Kelvin wave is found around 40-m depth on 1 January. This could be due to the significant contribution of higher vertical modes to the velocity fields, indicating that the SSH signal associated with coastal Kelvin wave is not sufficient to deduce the velocity. As indicated in previous observational studies, the maximum alongshore velocity associated with the Kelvin wave propagation often occurs at subsurface (e.g., Drushka et al. 2010). Although locations of these observations are mostly around or east of the Lombok Strait or within the Indonesian seas (Drushka et al. 2010; Pujiana et al. 2013), the model result is consistent with the observed structure. On 6 January, the maximum of alongshore velocity is found at the surface. This could be due to the interaction between active eddies and Kelvin wave propagation.

It should be noted that the Kelvin wave propagation can be found more clearly in the coarse-resolution model because of the weak mesoscale eddy activity in the model (e.g., Shinoda et al. 2012). However, the weaker eddy activity in this region in the model may not be realistic, and furthermore it is possible that the Kelvin wave propagation could be influenced by strong eddy activity as a result of the nonlinear interaction. Hence, the use of the high-resolution model is crucial to examine the processes such as Kelvin wave propagation not only by adequately resolving narrow straits but also by generating realistic eddies. Accordingly, processes found in coarse-resolution models must be reexamined using eddy-resolving models, particularly during the season of strong eddy activity.

5. Discussion

While the result shown in Fig. 16 clearly demonstrates the remote influence of equatorial winds in the Indian Ocean

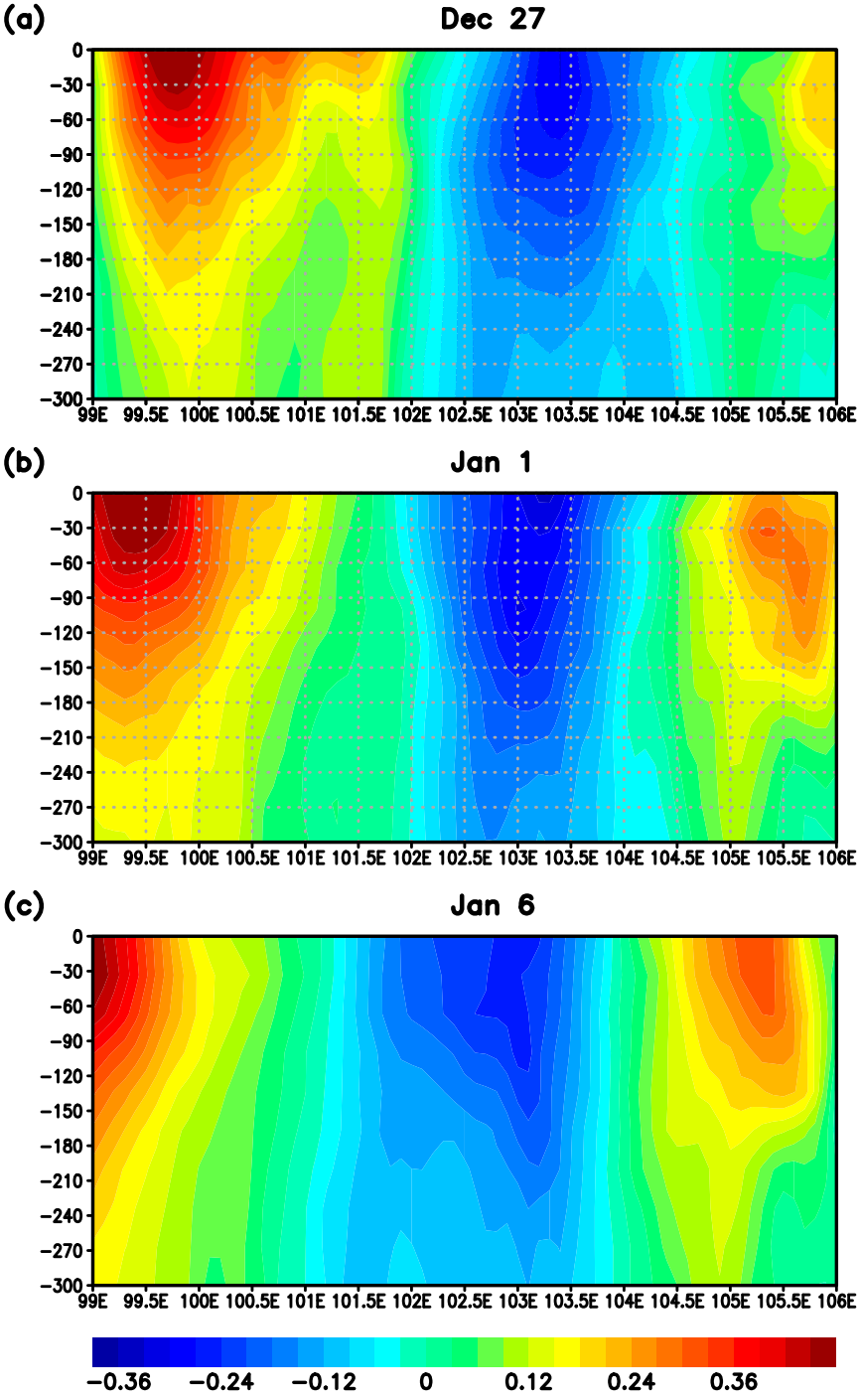

FIG. 19. Vertical cross sections (upper 300 m) of the alongshore velocity ($m\,s^{-1}$) along the white line in Fig. 18 for the periods (a) 27 December 2011 and (b) 1 and (c) 6 January 2012. The alongshore velocity is defined as a velocity component perpendicular to the white line.

on the ITF, processes within the Indonesian seas (e.g., local wind; Fig. 17) may affect the ITF variability during this period. To examine the influence of local winds, variability of surface winds in the Indonesian seas during the period of large ITF variability is described. Figure 20 shows the time series of zonal and meridional surface winds in the Makassar Strait during December 2011–January 2012, which covers the period of the rapid reduction and acceleration of the ITF. While a significant variation of surface winds on the time scale of 5–8 days is evident in both zonal

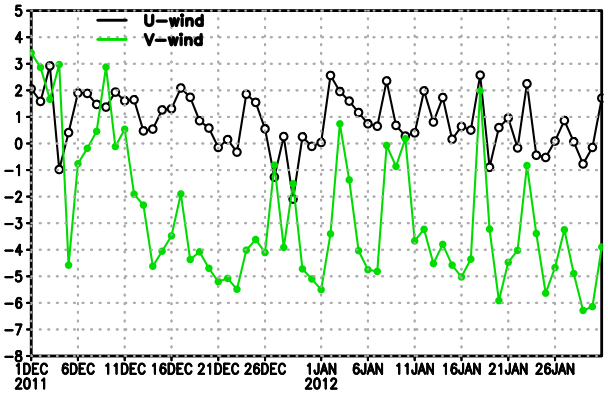

FIG. 20. Zonal (black line) and meridional (green line) winds ($m\,s^{-1}$) at 10-m height in the Makassar Strait (2.88°S, 118.5°E).

and meridional winds, any local wind changes that possibly could cause the rapid acceleration and decay in the Makassar Strait during this period are not evident in the time series. We further examine the time series of other locations between the Lombok Strait and the Makassar Strait. The variation of the winds in those two locations is similar, and again no evidence is found for any significant contribution from surface winds that can locally drive the rapid changes of meridional currents.

As shown in Fig. 17, strong surface winds associated with the MJO propagation are evident within the Java Sea. Figure 21 shows surface current anomalies within Indonesian seas during late December–early January when strong zonal winds are observed in the Java Sea. In late December, northeastward currents are evident in the western and middle parts of Java Sea, which are associated with SSH gradients. These SSH and surface current anomalies move eastward, and anomalous northward currents are found between Kalimantan and Sulawesi in early January. This suggests that anomalous SSH and currents in the Java Sea propagate eastward and may contribute to surface currents along the Makassar Strait. Although most areas of the Java Sea are very shallow, the variability propagated from the Java Sea may contribute significantly to velocity variations in the upper 100 m during this period.

While local winds in the Java Sea could generate currents toward the south coast of Kalimantan (Fig. 17), a portion of SSH anomalies propagate from north of the Karimata Strait (Figs. 14 and 21), and thus part of the anomalous SSH and currents in the Java Sea could be originally generated in the remote area in the South China Sea. The relative contribution of local winds to anomalous currents in the Java Sea during this period, however, is difficult to quantify. Although a possible impact of currents and SSH variations in the Java Sea on the Makassar Strait throughflow is consistent with previous studies (Gordon et al. 2003; Fang et al. 2010; Susanto et al. 2013), model experiments with different configurations (e.g., Tozuka et al. 2007) are necessary to isolate and further quantify the impact.

Previous studies suggest that ITF variability could influence regional precipitation and atmospheric circulations over the Maritime Continent through SST changes (e.g., Sprintall et al. 2014). The analysis of the model output in this study demonstrates that the strong equatorial jets generated by the MJO-induced surface winds influence the upper-ocean variability within the Indonesian seas as a result of wave propagation, and thus MJO events could generate significant anomalous near-surface currents in the ITF region. As SST in this region could strongly influence rainfall characteristics over the Maritime Continent and in turn could impact the global atmospheric circulation (e.g., Chang and Lau 1982; Sardeshmukh and Hoskins 1988), one of the key issues concerning ITF variability is whether the anomalous currents remotely produced by the MJO could generate significant SST changes in this region. Figure 22 shows anomalous upper-ocean currents in the Indonesian seas produced by the MJO events during DYNAMO along with SST in the same period from the model and two different SST analyses. In the model, there are strong north–south SST gradients in the southern part of the Java Sea around 7°S because of the relatively cold waters near the islands. As a result, the anomalous northward currents cross areas of strong SST gradients. Also, there are strong SST gradients between the shallow shelf region and the deeper open ocean areas (see Fig. 1 for the topography). The warmer waters in the shelf region extend near the west coast of Sulawesi around the Makassar Strait and create strong SST gradient areas where the anomalous northward currents cross. The SST changes in these areas, which exceed 1°C within the distance of 1° longitude/latitude, suggest that anomalous currents generate significant heat advection in this region, which in turn affects the SST. A similar magnitude of north–south SST gradient along the current path is found in the high-resolution SST analysis (Fig. 22, center), but the location is farther north (around 3.5°S). The spatial pattern of SST from another SST analysis (Reynolds et al. 2007) is similar to the model in which the SST contrast between the shelf region and open ocean areas is evident, but the SST gradient is not as sharp as in the model. Yet the magnitude of the SST gradient along the path of anomalous current is still substantial.

The strong SST gradient within the Indonesian seas, which is comparable to the one shown in Fig. 22, is often found in the model and high-resolution SST analysis at other times (not shown). This suggests that current anomalies on the subseasonal time scale could significantly influence the SST in the Indonesian seas. During DYNAMO, the northward current at the

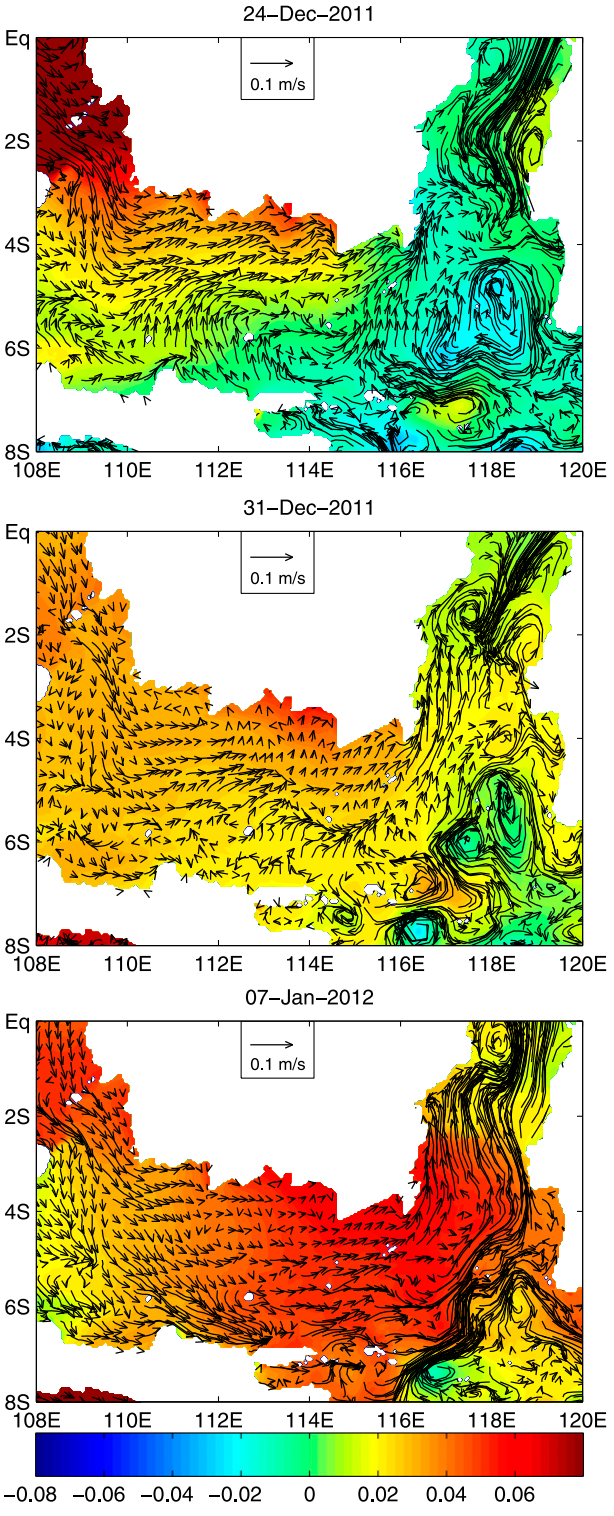

FIG. 21. SSH (shading; m) and surface velocity anomalies (vectors) during (top) 24 and (middle) 31 December 2011 and (bottom) 7 January 2012 relative to the mean of December 2011–January 2012 from the HYCOM simulation. A 10-day running filter has been applied to the time series.

Makassar Strait exceeded 0.5 m s^{-1}, and thus it is likely that it caused significant SST changes in the Indonesian seas and possibly influenced the local atmospheric convection. In addition to SST changes in the Makassar Strait, the variation of anomalous surface currents in the entire Java Sea and Banda Sea during this time is significant (not shown), and it could influence SSTs in large areas within the Indonesian seas.

Accurate SST and upper-ocean temperature data that resolve subseasonal or shorter time scales are necessary to quantify the impact of anomalous currents produced by the MJO on SST changes over the Maritime Continent. For the purpose of improving our understanding the role of the Maritime Continent in the global weather–climate continuum, the international field campaign the Year of the Maritime Continent (YMC), which includes the intensive atmospheric and ocean observations in the Indonesian seas region, is currently being planned. In particular, a plan for the ocean component of the YMC will be detailed in the next few years, and the results of ocean modeling, such as this study, will hopefully provide the useful information for the improvement of the current YMC plans.

6. Summary

The CINDY/DYNAMO international field campaign was conducted in boreal fall 2011 and winter 2011/12 with the goal of advancing our understanding of key processes for the MJO initiation and improving MJO prediction. Upper-ocean variability associated with the MJO events during the field campaign was well monitored by a variety of observations, including an array of enhanced surface moorings deployed in the central tropical Indian Ocean. During the field campaign, three active episodes of large-scale atmospheric convection and anomalous surface zonal winds associated with the MJO propagated eastward across the tropical Indian Ocean (Yoneyama et al. 2013). The second and third MJO events, which were initiated in the Indian Ocean in late November and mid-December, are unique in that two strong episodes of atmospheric convection occurred within one month without a clear suppressed phase between the events. Satellite observations indicate that these MJO events generated a strong ocean response that includes intense equatorial oceanic jets with a large zonal extent (~40°). It is possible that such strong upper-ocean variability could significantly influence remote areas including the Indonesian seas and the Indonesian Throughflow (ITF).

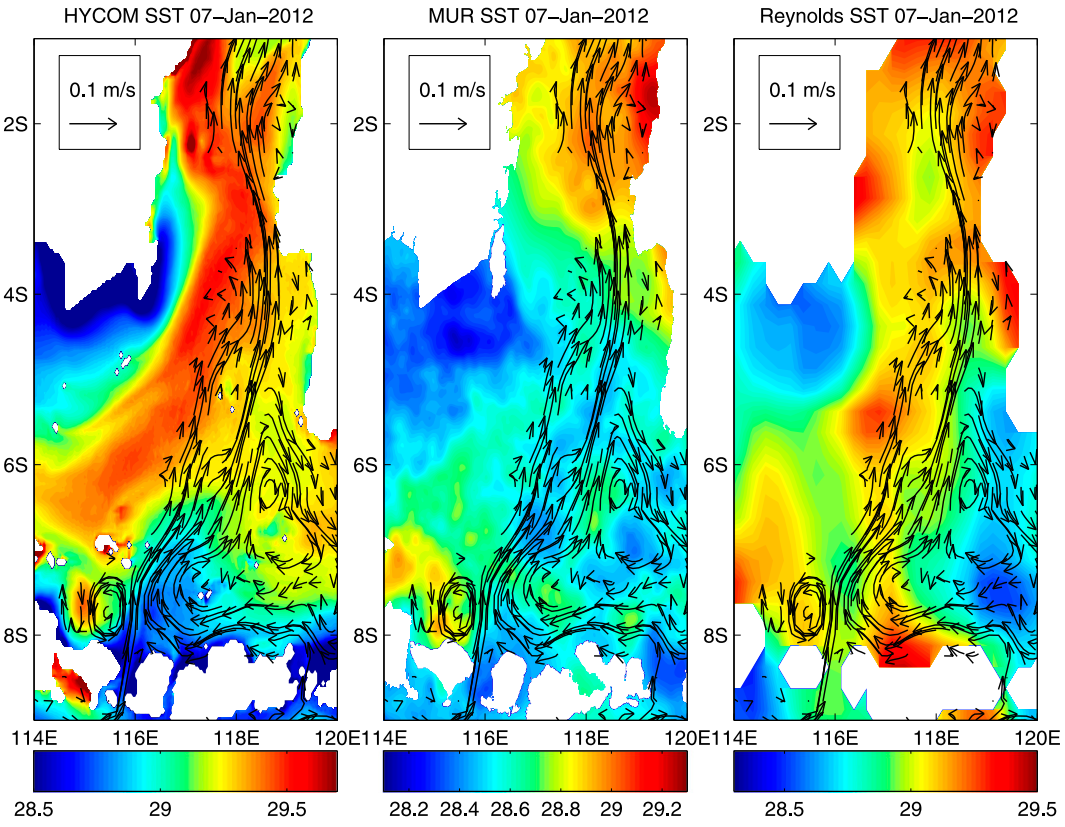

FIG. 22. As in Fig. 15, but for average velocity in the upper 100 m and SST (shading; °C) on 7 January 2012 from (left) HYCOM simulation, (center) MUR, and (right) Reynolds et al. (2007). A 30-day running filter has been applied to the SST time series. The total range of the color bar for all panels is 1.2°C, but the SST values of each color are different in each panel.

In this study, the influence of the unique MJO events during the DYNAMO on ITF variability is investigated using a high-resolution (1/25°) global ocean general circulation model (HYCOM). In particular, the large-scale upper-ocean velocity variability associated with Kelvin wave propagation, which was not emphasized in previous studies, is examined based on the model simulation. The model results are first compared with the data collected during DYNAMO, showing that the global HYCOM is able to realistically simulate the strong equatorial jets generated by surface forcing fields associated with the MJO events. Our results suggest that strong equatorial jets with a large zonal extent lasted more than one month in late November 2011–early January 2012. A large increase in SSH (and thus deepening of the thermocline) along the eastern boundary is found in late December. Further analysis of the model simulation demonstrates that the SSH and alongshore velocity anomalies at the eastern boundary propagate along the coast of Sumatra and Java as coastal Kelvin waves, which largely reduces the ITF transport at the Makassar Strait during January–early February, although local wind-induced Ekman transports may also have some contributions. It is found that alongshore velocity anomalies associated with the Kelvin wave propagation significantly lead SSH anomalies, likely resulting from the effects of lateral friction and Ekman transports driven by local winds. The magnitude of the anomalous currents associated with the Kelvin wave propagation is comparable to that associated with the seasonal variation, and thus the typical seasonal cycle of ITF could be largely altered by strong MJO events such as those observed during the CINDY/DYNAMO field campaign.

Acknowledgments. The TAO Project Office of NOAA/PMEL provided the RAMA mooring time series data (http://www.pmel.noaa.gov/tao/rama). The altimeter products are produced by SSALTO/DUACS and are distributed by AVISO. Blended SST product is provided by the NOAA/OAR/ESRL PSD. MUR SST product is obtained from NASA JPL site (http://mur.jpl.nasa.gov). The OSCAR Project Office has made the

surface velocity data available. Grants of computer time for the modeling work were provided by the Department of Defense (DoD) High Performance Computing Modernization Program and the simulations were performed on the IBM iDataPlex (Haise) at the Navy DoD Supercomputing Resources Center, Stennis Space Center, Mississippi. Computing resources were also provided by the Climate Simulation Laboratory at NCAR's Computational and Information Systems Laboratory, sponsored by the National Science Foundation and other agencies, as well as Texas A&M University High Performance Research Computing. Constructive comments from the reviewers are gratefully acknowledged. This research is supported by NOAA Grant NA15OAR431074, NSF Grant AGS-1347132, and an ONR/LASP grant under Program Element 601153. W. Han is supported by NASA OVWST Award NNX14AM68G. R.-C. Lien is supported by NSF Grant OCE-1029488. This paper has been approved for public release and distribution is unlimited.

REFERENCES

Bleck, R., 2002: An oceanic general circulation model framed in hybrid isopycnic-Cartesian coordinates. *Ocean Modell.*, **4**, 55–88, doi:10.1016/S1463-5003(01)00012-9.

Carnes, M. R., R. W. Helber, C. N. Barron, and J. M. Dastugue, 2010: Validation test report for GDEM4. Naval Research Laboratory Memo. NRL/MR/7330-10-9271, 59 pp. [Available online at http://www7320.nrlssc.navy.mil/pubs/2010/gdem4-2010.pdf.]

Chang, C.-P., and K. M. Lau, 1982: Short-term planetary-scale interactions over the tropics and midlatitudes during northern winter. Part I: Contrasts between active and inactive periods. *Mon. Wea. Rev.*, **110**, 933–946, doi:10.1175/1520-0493(1982)110<0933:STPSIO>2.0.CO;2.

Chassignet, E. P., L. T. Smith, G. R. Haliwell, and R. Bleck, 2003: North Atlantic simulations with the Hybrid Coordinate Ocean Model (HYCOM): Impact of the vertical coordinate choice, reference pressure, and thermobaricity. *J. Phys. Oceanogr.*, **33**, 2504–2526, doi:10.1175/1520-0485(2003)033<2504:NASWTH>2.0.CO;2.

Chi, N.-H., R.-C. Lien, E. A. D'Asaro, and B. B. Ma, 2014: The surface mixed layer heat budget from mooring observations in the central Indian Ocean during Madden–Julian oscillation events. *J. Geophys. Res. Oceans*, **119**, 4638–4652, doi:10.1002/2014JC010192.

Clarke, A. J., and X. Liu, 1993: Observations and dynamics of semiannual and annual sea levels near the eastern equatorial Indian Ocean boundary. *J. Phys. Oceanogr.*, **23**, 386–399, doi:10.1175/1520-0485(1993)023<0386:OADOSA>2.0.CO;2.

Cravatte, S., J. Picaut, and G. Eldin, 2003: Second and first baroclinic Kelvin modes in the equatorial Pacific at intraseasonal time scales. *J. Geophys. Res.*, **108**, 3266, doi:10.1029/2002JC001511.

Drushka, K., J. Sprintall, S. Gille, and I. Brodjonegoro, 2010: Vertical structure of Kelvin waves in the Indonesian Throughflow exit passages. *J. Phys. Oceanogr.*, **40**, 1965–1987, doi:10.1175/2010JPO4380.1.

Durland, T. S., and B. Qiu, 2003: Transmission of subinertial Kelvin waves through a strait. *J. Phys. Oceanogr.*, **33**, 1337–1350, doi:10.1175/1520-0485(2003)033<1337:TOSKWT>2.0.CO;2.

Fairall, C., E. F. Bradley, D. P. Rogers, J. B. Edson, and G. S. Young, 1996: The TOGA COARE bulk flux algorithm. *J. Geophys. Res.*, **101**, 3747–3764, doi:10.1029/95JC03205.

——, ——, J. E. Hare, A. A. Grachev, and J. B. Edson, 2003: Bulk parameterization of air–sea fluxes: Updates and verification for the COARE algorithm. *J. Climate*, **16**, 571–591, doi:10.1175/1520-0442(2003)016<0571:BPOASF>2.0.CO;2.

Fang, G., and Coauthors, 2010: Volume, heat, and freshwater transports from the South China Sea to Indonesian seas in the boreal winter of 2007–2008. *J. Geophys. Res.*, **115**, C12020, doi:10.1029/2010JC006225.

Feng, M., and S. Wijffels, 2002: Intraseasonal variability in the South Equatorial Current of the east Indian Ocean. *J. Phys. Oceanogr.*, **32**, 265–277, doi:10.1175/1520-0485(2002)032<0265:IVITSE>2.0.CO;2.

Gaiser, P. W., and Coauthors, 2004: The WindSat spaceborne polarimetric microwave radiometer: Sensor description and early orbit performance. *IEEE Trans. Geosci. Remote Sens.*, **42**, 2347–2361, doi:10.1109/TGRS.2004.836867.

Gordon, A. L., 2005: Oceanography of the Indonesian seas and their throughflow. *Oceanography*, **18**, 14–27, doi:10.5670/oceanog.2005.01.

——, R. D. Susanto, and K. Vranes, 2003: Cool Indonesian Throughflow as a consequence of restricted surface layer flow. *Nature*, **425**, 824–828, doi:10.1038/nature02038.

——, ——, A. Feld, B. A. Huber, W. Pranowo, and S. Wirasantosa, 2008: Makassar Strait Throughflow 2004 to 2006. *Geophys. Res. Lett.*, **35**, L24605, doi:10.1029/2008GL036372.

Gottschalck, J., P. Roundy, C. Schreck, A. Vintzileos, and C. Zhang, 2013: Large-scale atmospheric and oceanic conditions during the 2011–12 DYNAMO field campaign. *Mon. Wea. Rev.*, **141**, 4173–4196, doi:10.1175/MWR-D-13-00022.1.

Han, W., 2005: Origins and dynamics of the 90-day and 30–60-day variations in the equatorial Indian Ocean. *J. Phys. Oceanogr.*, **35**, 708–728, doi:10.1175/JPO2725.1.

——, J. P. McCreary Jr., D. L. T. Anderson, and A. J. Mariano, 1999: On the dynamics of the eastward surface jets in the equatorial Indian Ocean. *J. Phys. Oceanogr.*, **29**, 2191–2209, doi:10.1175/1520-0485(1999)029<2191:DOTESJ>2.0.CO;2.

Hurlburt, H. E., E. J. Metzger, J. Sprintall, S. N. Riedlinger, R. A. Arnone, T. Shinoda, and X. Xu, 2011: Circulation in the Philippine Archipelago simulated by 1/12° and 1/25° global HYCOM and EAS NCOM. *Oceanography*, **24**, 28–47, doi:10.5670/oceanog.2011.02.

Jensen, T. G., 1993: Equatorial variability and resonance in a wind-driven Indian Ocean model. *J. Geophys. Res.*, **98**, 22 533–22 552, doi:10.1029/93JC02565.

——, T. Shinoda, S. Chen, and M. Flatau, 2015: Ocean response to CINDY/DYNAMO MJOs in air-sea coupled COAMPS. *J. Meteor. Soc. Japan*, **93A**, 157–178, doi:10.2151/jmsj.2015-049.

Kållberg, P., A. Simmons, S. Uppala, and M. Fuentes, 2004: The ERA-40 archive. ERA-40 Project Rep. Series 17, 31 pp. [Available online at http://mms.dkrz.de/pdf/klimadaten/projects/era40/e40Archive.pdf.]

Kara, A. B., A. J. Wallcraft, P. J. Martin, and R. L. Pauley, 2009: Optimizing surface winds using QuikSCAT measurements in the Mediterranean Sea during 2000–2006. *J. Mar. Syst.*, **78**, 119–131, doi:10.1016/j.jmarsys.2009.01.020.

Kessler, W. S., M. J. McPhaden, and K. M. Weickmann, 1995: Forcing of intraseasonal Kelvin waves in the equatorial Pacific Ocean. *J. Geophys. Res.*, **100**, 10 613–10 631, doi:10.1029/95JC00382.

Lagerloef, G. S. E., G. Mitchum, R. Lukas, and P. Niiler, 1999: Tropical Pacific near surface currents estimated from altimeter,

wind and drifter data. *J. Geophys. Res.*, **104**, 23 313–23 326, doi:10.1029/1999JC900197.

Large, W. G., J. C. McWilliams, and S. C. Doney, 1994: Oceanic vertical mixing: A review and a model with a nonlocal boundary layer parameterization. *Rev. Geophys.*, **32**, 363–403, doi:10.1029/94RG01872.

Lee, T., I. Fukumori, D. Menemenlis, Z. Xing, and L. Fu, 2002: Effects of the Indonesian Throughflow on the Pacific and Indian Oceans. *J. Phys. Oceanogr.*, **32**, 1404–1429, doi:10.1175/1520-0485(2002)032<1404:EOTITO>2.0.CO;2.

Masumoto, Y., and T. Yamagata, 1993: Simulated seasonal circulation in the Indonesian Seas. *J. Geophys. Res.*, **98**, 12 501–12 509, doi:10.1029/93JC01025.

McPhaden, M. J., and Coauthors, 2009: RAMA: The Research Moored Array for African–Asian–Australian Monsoon Analysis and Prediction. *Bull. Amer. Meteor. Soc.*, **90**, 459–480, doi:10.1175/2008BAMS2608.1.

Metzger, E. J., H. E. Hurlburt, X. Xu, J. F. Shriver, A. L. Gordon, J. Sprintall, R. D. Susanto, and H. M. van Aken, 2010: Simulated and observed circulation in the Indonesian Seas: 1/12° global HYCOM and the INSTANT observations. *Dyn. Atmos. Oceans*, **50**, 275–300, doi:10.1016/j.dynatmoce.2010.04.002.

Molinari, R. L., D. Olson, and G. Reverdin, 1990: Surface current distributions in the tropical Indian Ocean derived from compilations of surface buoy trajectories. *J. Geophys. Res.*, **95**, 7217–7238, doi:10.1029/JC095iC05p07217.

Moore, D. W., and J. P. McCreary, 1990: Excitation of intermediate frequency equatorial waves at a western ocean boundary: With application to observations from the western Indian Ocean. *J. Geophys. Res.*, **95**, 5219–5231, doi:10.1029/JC095iC04p05219.

Moum, J. N., and Coauthors, 2013: Air–sea interactions from westerly wind bursts during the November 2011 MJO in the Indian Ocean. *Bull. Amer. Meteor. Soc.*, **95**, 1185–1199, doi:10.1175/BAMS-D-12-00225.1.

Nagura, M., and M. J. McPhaden, 2010: Wyrtki Jet dynamics: Seasonal variability. *J. Geophys. Res.*, **115**, C07009, doi:10.1029/2009JC005922.

Pujiana, K., A. L. Gordon, and J. Sprintall, 2013: Intraseasonal Kelvin waves in Makassar Strait. *J. Geophys. Res. Oceans*, **118**, 2023–2034, doi:10.1002/jgrc.20069.

Qiu, B., M. Mao, and Y. Kashino, 1999: Intraseasonal variability in the Indo-Pacific Throughflow and the regions surrounding the Indonesian seas. *J. Phys. Oceanogr.*, **29**, 1599–1618, doi:10.1175/1520-0485(1999)029<1599:IVITIP>2.0.CO;2.

Qiu, Y., L. Li, and W. Yu, 2009: Behavior of the Wyrtki Jet observed with surface drifting buoys and satellite altimeter. *Geophys. Res. Lett.*, **36**, L18607, doi:10.1029/2009GL039120.

Ralph, E. A., K. Bi, and P. P. Niiler, 1997: A Lagrangian description of the western equatorial Pacific response to the wind burst of December 1992. *J. Climate*, **10**, 1706–1721, doi:10.1175/1520-0442(1997)010<1706:ALDOTW>2.0.CO;2.

Reynolds, R. W., T. M. Smith, C. Liu, D. B. Chelton, K. S. Casey, and M. G. Schlax, 2007: Daily high-resolution-blended analyses for sea surface temperature. *J. Climate*, **20**, 5473–5496, doi:10.1175/2007JCLI1824.1.

Rosmond, T. E., J. Teixeira, M. Peng, T. F. Hogan, and R. Pauley, 2002: Navy Operational Global Atmospheric Prediction System: Forcing for ocean models. *Oceanography*, **15**, 99–108, doi:10.5670/oceanog.2002.40.

Roundy, P. E., and G. N. Kiladis, 2006: Observed relationships between oceanic Kelvin waves and atmospheric forcing. *J. Climate*, **19**, 5253–5272, doi:10.1175/JCLI3893.1.

Sardeshmukh, P. D., and B. J. Hoskins, 1988: The generation of global rotational flow by steady idealized tropical divergence. *J. Atmos. Sci.*, **45**, 1228–1251, doi:10.1175/1520-0469(1988)045<1228:TGOGRF>2.0.CO;2.

Schiller, A., S. E. Wijffels, J. Sprintall, R. Molcard, and P. R. Oke, 2010: Pathways of intraseasonal variability in the Indonesian Throughflow region. *Dyn. Atmos. Oceans*, **50**, 174–200, doi:10.1016/j.dynatmoce.2010.02.003.

Shinoda, T., and H. H. Hendon, 2001: Upper-ocean heat budget in response to the Madden–Julian oscillation in the western equatorial Pacific. *J. Climate*, **14**, 4147–4165, doi:10.1175/1520-0442(2001)014<4147:UOHBIR>2.0.CO;2.

——, P. E. Roundy, and G. N. Kiladis, 2008: Variability of intraseasonal Kelvin waves in the equatorial Pacific Ocean. *J. Phys. Oceanogr.*, **38**, 921–944, doi:10.1175/2007JPO3815.1.

——, W. Han, E. J. Metzger, and H. Hurlburt, 2012: Seasonal variation of the Indonesian Throughflow in Makassar Strait. *J. Phys. Oceanogr.*, **42**, 1099–1123, doi:10.1175/JPO-D-11-0120.1.

——, T. G. Jensen, M. Flatau, and S. Chen, 2013a: Surface wind and upper-ocean variability associated with the Madden–Julian oscillation simulated by the Coupled Ocean–Atmosphere Mesoscale Prediction System (COAMPS). *Mon. Wea. Rev.*, **141**, 2290–2307, doi:10.1175/MWR-D-12-00273.1.

——, ——, ——, ——, W. Han, and C. Wang, 2013b: Large-scale oceanic variability associated with the Madden–Julian oscillation during the CINDY/DYNAMO field campaign from satellite observations. *Remote Sens.*, **5**, 2072–2092, doi:10.3390/rs5052072.

Sprintall, J., A. L. Gordon, R. Murtugudde, and R. D. Susanto, 2000: A semiannual Indian Ocean forced Kelvin wave observed in the Indonesian seas in May 1997. *J. Geophys. Res.*, **105**, 17 217–17 230, doi:10.1029/2000JC900065.

——, and Coauthors, 2004: INSTANT: A new international array to measure the Indonesian Throughflow. *Eos, Trans. Amer. Geophys. Union*, **85**, 369–376, doi:10.1029/2004EO390002.

——, S. Wijffels, R. Molcard, and I. Jaya, 2009: Direct estimates of Indonesian Throughflow entering the Indian Ocean: 2004–2006. *J. Geophys. Res.*, **114**, C07001, doi:10.1029/2008JC005257.

——, A. L. Gordon, A. Koch-Larrouy, T. Lee, J. T. Potemra, K. Pujiana, and S. E. Wijffels, 2014: The Indonesian Seas and their role in the coupled ocean–climate system. *Nat. Geosci.*, **7**, 487–492, doi:10.1038/ngeo2188.

Susanto, D. W., and Y. T. Song, 2015: Indonesian Throughflow proxy from satellite altimeters and gravimeters. *J. Geophys. Res. Oceans*, **120**, 2844–2855, doi:10.1002/2014JC010382.

Susanto, R. D., A. Ffield, A. Gordon, and T. R. Adi, 2012: Variability of Indonesian Throughflow with Makassar Strait, 2004–2009. *J. Geophys. Res.*, **117**, C09013, doi:10.1029/2012JC008096.

——, Z. Wei, T. R. Adi, B. Fan, S. Li, and G. Fang, 2013: Observations of the Karimata Strait Throughflow from December 2007 to November 2008. *Acta Oceanol. Sin.*, **32**, 1–6, doi:10.1007/s13131-013-0307-3.

Tilburg, C. E., H. E. Hurlburt, J. J. O'Brien, and J. F. Shriver, 2001: The dynamics of the East Australian Current system: The Tasman Front, the East Auckland Current, and the East Cape Current. *J. Phys. Oceanogr.*, **31**, 2917–2943, doi:10.1175/1520-0485(2001)031<2917:TDOTEA>2.0.CO;2.

Tozuka, T., T. Qu, and T. Yamagata, 2007: Dramatic impact of the South China Sea on the Indonesian Throughflow. *Geophys. Res. Lett.*, **34**, L12612, doi:10.1029/2007GL030420.

Waliser, D. E., R. Murtugudde, and L. Lucas, 2003: Indo-Pacific Ocean response to atmospheric intraseasonal variability.

Part I: Austral summer and the Madden–Julian oscillation. *J. Geophys. Res.*, **108**, 3160, doi:10.1029/2002JC001620.

Wheeler, M., and H. Hendon, 2004: An all-season real-time multivariate MJO index: Development of an index for monitoring and prediction. *Mon. Wea. Rev.*, **132**, 1917–1932, doi:10.1175/1520-0493(2004)132<1917:AARMMI>2.0.CO;2.

Wyrtki, K., 1973: An equatorial jet in the Indian Ocean. *Science*, **181**, 262–264, doi:10.1126/science.181.4096.262.

Yoneyama, K., C. Zhang, and C. N. Long, 2013: Tracking pulses of the Madden–Julian oscillation. *Bull. Amer. Meteor. Soc.*, **94**, 1871–1891, doi:10.1175/BAMS-D-12-00157.1.

Yu, Z., and J. T. Potemra, 2006: Generation mechanism for the intraseasonal variability in the Indo-Australian basin. *J. Geophys. Res.*, **111**, C01013, doi:10.1029/2005JC003023.

Zhang, C., J. Gottschalck, E. D. Maloney, M. W. Moncrieff, F. Vitart, D. E. Waliser, B. Wang, and M. C. Wheeler, 2013: Cracking the MJO nut. *Geophys. Res. Lett.*, **40**, 1223–1230, doi:10.1002/grl.50244.

Zhou, L., and R. Murtugudde, 2010: Influences of Madden–Julian oscillations on the eastern Indian Ocean and the Maritime Continent. *Dyn. Atmos. Oceans*, **50**, 257–274, doi:10.1016/j.dynatmoce.2009.12.003.